INVESTIGATION OF HEAT THERAPIES USING MULTI-SCALE MODELS AND STATISTICAL METHODS

HUANG WEI HSUAN
B.Eng (Hons.), NUS

A THESIS SUBMITTED

FOR THE DEGREE OF DOCTOR OF PHILOSOPHY

DEPARTMENT OF MECHANICAL ENGINEERING

NATIONAL UNVERSITY OF SINGAPORE

2013

DECLARATION

I hereby declare that the thesis is my original work and it has been written by me in its entirety. I have duly acknowledged all the sources of information which have been used in the thesis.

This thesis has also not been submitted for any degree in any university previously.

_____

Huang Wei Hsuan
14 January 2013

Acknowledgement

I would like to express my gratitude to my supervisors, Asst. Professor CHUI Chee Kong from the Department of Mechanical Engineering, NUS and Assoc. Professor CHANG KY Stephen from the Department of Surgery. Without their guidance and mentorship, it would not have been possible for me to accomplish such interdisciplinary work. I also like to thank Professor KOBAYAHSHI Etsuko from University of Tokyo for her support in JSPS.

I would also like to thank the people from my research group and members of my lab, Control and Mechatronics Lab 1, including Mr. WEN Rong (ME,NUS), Mr. YANG Liang Jing (ME,NUS), Mr. CHNG Chin Boon (ME,NUS), Mr. LEE Chun Xiong (ME,NUS), Mr. XIONG Linfei (ME,NUS), Mr. FU Yabo (ME, NUS), Ms. WU Zimei (ME,NUS), Dr. NGUYEN Phu binh (ECE, NUS), and many others.

Last but not least, I'll like to thank my family (Dad, Mom and Sister), friends and loved ones for their support. Without their consideration and endless supports, I would not be able to devote myself fully to the PhD program.

Table of Contents

SUMMARY

Radio-frequency (RF) ablation is commonly used for hepatic carcinoma or liver tumor treatment due to its minimal invasiveness and simplicity. RF ablation is the application of a high frequency (550KHz) electric voltage within a target biological tissue which generates high current density and hence ionic agitation and frictional heating. The increase in temperature leads to coagulative necrosis in liver tissue or tumor.

Understanding the *science of ablation* is valuable for hyperthermia treatment. It is useful in predicting the outcome of RF ablation, minimizing healthy tissue damage and optimizing RF ablation procedure. Quantifying heat transfer for RF ablation can be achieved by Penne's bioheat equation, which is a partial differential equation relating Specific Adsorption Rate (SAR) power to temperature. The Penne's bioheat equation can be solved using finite element method with input comprising tissue material properties such as heat transfer coefficient, conductivity, etc.

Tissue impedance plays an important role in the simulation of RF ablation, due to the dependence of joule heating on conductivity. A multi-scale geometrical impedance model was proposed to mimic the impedance dispersion of liver tissue. This model is built from cellular scale and scaled upwards to liver lobule level and finally the tissue level. The model is able to model differences in blood flow in the tissue which can be useful in blood detection technologies. The theoretical model matches the impedance dispersion data better than that of the classic Cole-Cole model with *sound physiological explanation*.

RF ablation results in tissue injury causing changes in tissue cellular structures at micro level, and its physical properties at macro level. The relationship between tissue

mechanical properties and ablation was studied. Liver tissue stiffness is larger for ablated tissue at small strains, and eventually leveled when strain increases, exhibiting viscoelastic properties. A novel 3D plot was used to illustrate the relationship between tissue stress-strain relationship, tissue bulk electrical impedance and ablation time. The plot *correlates the relationship between tissue injury and changes in physical properties*.

RF ablation has been used clinically for liver tumor ablation. However, there is a limitation for large tumor (3~8cm in diameter) ablation which requires multiple electrode insertion and ablation. Surgical planning is important in determining the appropriate overlapping of RF ablation to prevent relapse while minimizing healthy tissue damages. A *novel Stochastic Finite Element* (SFE) method was incorporated into large tumor RF ablation surgical planning. Due to variation in tissue properties and sample variations, stochastic FE method was proposed for a non-deterministic simulation result.

Liver resection remains the gold standard in liver cancer treatment, and RF ablation has been used to assist liver resection surgery (hepatectomy) to minimize blood losses during surgery. RF is used to coagulate blood vessels in prevention of bleeding during surgical resection. An integrated RF ablation and resection laparoscopic device was designed and fabricated to overcome difficulties faced during tissue division in laparoscopy surgery. The device was tested in-vivo on a porcine model with a Laser Doppler sensor integrated for blood flow detection. The device was able to detect the presence of blood prior to resection and informs the user with the help of a Graphic User Interface created on a PC. Results from the device show competitiveness with existing commercial products in both operation time and less blood losses.

LIST OF FIGURES

ABBREVIATIONS

Chapter 1

INTRODUCTION

Hyperthermia therapies are commonly used for cancer treatment. These therapies involve an elevation in tissue temperature (or reduction in the case of cryo-ablation) to induce cell necrosis in cancerous tumors. Temperature related tissue injuries are the basic mechanism present in hyperthermia treatments. These methods are effective due to the cytotoxicity observed in cells above a threshold temperature. In addition, S-phase cells which are the most ionizing radiation resistant are most sensitive to hyperthermia (Craciunescu 1999). There are many methods for energy deposition in hyperthermia treatment including Ultrasound ablation, Laser ablation, Radiofrequency ablation and Microwave ablation, etc. This thesis concentrates on Radio-Frequency (RF) ablation and mainly therapeutic treatments for hepatic malignancies.

In RF ablation, electrical pulses (~500 KHz) are used to induce Joule heating and necrosis to tissue and cancerous cells. The principle of RF ablation is to generate ionic agitation and frictional heating thus leading to coagulative necrosis in tissues. The electric field lines that are induced from the electrode tip by the applied voltage induce an electric force on the charged ions within the electrolytic medium of the liver tissue. This induced force produces a motion that causes ions in the tissue to rub against the surrounding fluid medium, causing friction and heating effect. The temperature at any point in the affected tissue zone is governed by the total frictional power input at the

point mediated by thermal conduction and a convective factor, which is primarily blood circulation.

The ultimate strategy of RF thermal tumor ablation therapy for hepatic and other malignancies has two main objectives (Adam 2009). Firstly, through the application of RF energy, the goal was to completely eradicate all malignant cells within a designated area. Based on clinical studies examining tumor progression for patients who underwent surgical resection procedure, and confirmation of viable malignant cells beyond visible tumor boundaries, tumor ablation therapies should attempt to include at least a 1.0cm "ablative" margin of seemingly normal tissue for liver. Secondly, while complete eradication of tumor is of primary importance, specificity and precision of RF therapy is also required. One significant advantage of RF thermal ablation over conventional standard surgical resection is the minimal blood losses and potential minimal amount of normal tissue damage/loss that occurs.

Tissue temperature distribution is an important study in understanding RF ablation. Penne's bioheat equation is the most commonly cited model for RF ablation modeling and can be solved with methods such as finite element analysis to prognosticate temperature distribution of ablated tissue. Tissue temperature can then be related to degrees of cell injury categorized into mass ablation, carbonization, water vaporization, protein denaturation and membrane dissociation (Thomsen 2009).

In general, an increase in temperature over a threshold, results in a change in tissue cell structure, cellular content, moisture loss and protein denaturalization. The change in structure leads to a change in mechanical properties due to skeletal changes in cells. Studies reported differences in mechanical property between native and thermally

damaged liver. In our experiments, observations were also made for ablation time, to be positively related to a change in tissue stiffness. Ablation time is a good approximation for tissue temperature, and quantitative relationship can be established between temperature and mechanical properties. Tissue injuries are often quantified in the micro scale by observing structures such as cells or their equivalent during necrosis. Optical and fluorescence characteristics of tissue, histochemical markers or Optical Coherence Tomography (OCT) are methods available for quantifying cell death (Lin 2003, Wierwille 2010). However, mechanical properties of tissue are observed in the macro level such as tissue level for most pragmatic purpose. Test rigs such as a compression machine, Magnetic Resonance Elastography (MRE) and ultrasound elastography are choices for quantifying mechanical properties both in-vivo and in-vitro. Relationship between tissue injury and tissue mechanical properties helps us relate the effect of an alteration of cell in a micro level (1 to 100 microns) on its macro level (1mm to 10cm) equivalent. A study of structural changes in the micro level, such as the skeletal structure of cells and extracellular matrix are often less commonplace in clinical practice, but only for specific interest groups.

Liver resection is the gold standard for hepatic carcinoma treatment. A new technique in liver resection was developed by Habib et al (2006) to synergize radio-frequency ablation and liver resection for significant reduction in blood losses during the resection procedure. Radio-frequency ablation was first performed on the desired line of resection on the liver and manual resection with surgical scalpel of the liver tissue follows thereafter. Radio-frequency was used to induce frictional heating in the healthy liver tissue and thus coagulation for minimizing blood loss during liver resection. The

technique also results in reduction of the length of the anesthetic time and the operating time. To achieve the effect of coagulation in normal liver parenchyma is much faster than that in tumor tissue. Coagulative necrosis in liver tumor tissue takes about 20 minutes for one probe application, but only 40 seconds to coagulate the same amount of normal liver tissue hence making the procedure very fast. The technique eliminates the need for intensive care unit facilities, and reduces the need to employ Pringle's maneuver (Milicevic 2008) which is often used for conventional tumor ablation for effective RF heating but results in ischemia-reperfusion hepatocellular injury. Ultimately, the technique results in less postoperative mortality and morbidity. However, there are some limitations to the Habib's technique. Firstly, Radio-Frequency energy should be applied carefully near the hilum or the vena cava because of its potential damaging effect on these structures. Secondly, healthy parenchymal tissue will be sacrificed for the resection procedure. However, the regenerative capacity of residual normal liver tissue should reduce the amount of potential damage by the technique. Thirdly, it is not possible for the surgeon to be sure of the complete coagulation of the tissue along the cutting plane. Hence, occasional blood losses will be encountered during operation.

A prototype was built to incorporate the Habib's technique into a single device, combining both procedures of radio-frequency ablation and hepatectomy. The prototype enables a smooth surgical procedure of a Habib procedure in a compact and integrated solution laparoscopically. It removes the need for switching between laparoscopic tools during the surgery thus saving significant time and effort. A Laser Doppler Flow (LDF) Sensor was integrated for blood flow detection after Radio-frequency ablation was

employed and is able to present real time graphical information to the surgeon during the surgery.

The motivation of this thesis is to understand the science of RF ablation - to be able to understand, model and simulate RF ablation, and to relate physical properties changes with RF ablation. By doing so, the knowledge can be used to design and build novel medical devices for their intended purpose. The several chapters in the thesis addresses existing limitation in physical or methodological modeling of topics relating to RF ablation with improved work that were also published.

This chapter introduces hyperthermia treatment with RF ablation and its applications. The second chapter of the thesis covers literature reviews for the various fields of RF ablation. This chapter provides background knowledge on the subsequent chapters. The third chapter covers work in bio-impedance modeling with the proposal of a geometry based, multi-scale model which models the frequency dispersion of hepatic tissue impedance. Bioimpedance is related to the effectiveness of RF ablation and the proposed model can be used in developing a blood sensing technology for the prototype discussed in chapter six. The fourth chapter covers work in modeling the change in tissue impedance due to RF ablation and the correlation between impedance, stiffness and ablation duration. This chapter is also related to the optimization of RF ablation and is applicable to chapter six. In chapter five, a statistical based stochastic finite element method was demonstrated in large tumor RF ablation planning. The relevant contribution of the thesis is discussed in chapter six in the building of a prototype device. The thesis is wrapped up finally in chapter seven with the conclusion and the future of RF ablation studies.

Chapter 2

LITERATURE REVIEW

This chapter reviews previous work in the field of Radio-frequency ablation as well as related work in multi-scale modeling and bioimpedance. First section covers the existing work in modeling RF ablation while the second section covers the mechanism of tissue injury due to RF ablation. The third and fourth section covers existing work in bioimpedance related to RF ablation and blood flow modeling. The fifth section covers a short description of multi-scale model, which is the main modeling technique used in the thesis. Lastly, statistical method in Finite Element analysis is briefly introduced.

2.1 Basics of RF ablation

Many forms of hyperthermia treatment exist in clinical practices -Radiofrequency (RF) ablation, Microwave ablation, Laser ablation, Ultrasonic ablation and Cryoablation. RF assisted methods have been widely used in the treatment for hepatocellular cancers, breast tumors and cardiology treatments. The increase in temperature leads to coagulative necrosis in tissue (Haemmerich 2003).

Catheters used for RF ablation are often needle electrodes for its high current density. Catheters can be found in two forms - monopolar or bipolar electrodes. Monopolar electrodes work on the principle of a single polarity electrode with a large grounding pad attached to patients. The current density is highest at the electrode tip-tissue interface where area of contact is small and decreases when current flows through

the body and exits from the grounding pad. Monopolar catheters enable electrode design to be small and slim, hence suitable for percutaneous or minimally invasive procedures. However due to the small area of contact, treatment area is limited. A possible way to increase treatment area is an expandable prong design which consists of retractable electrodes.

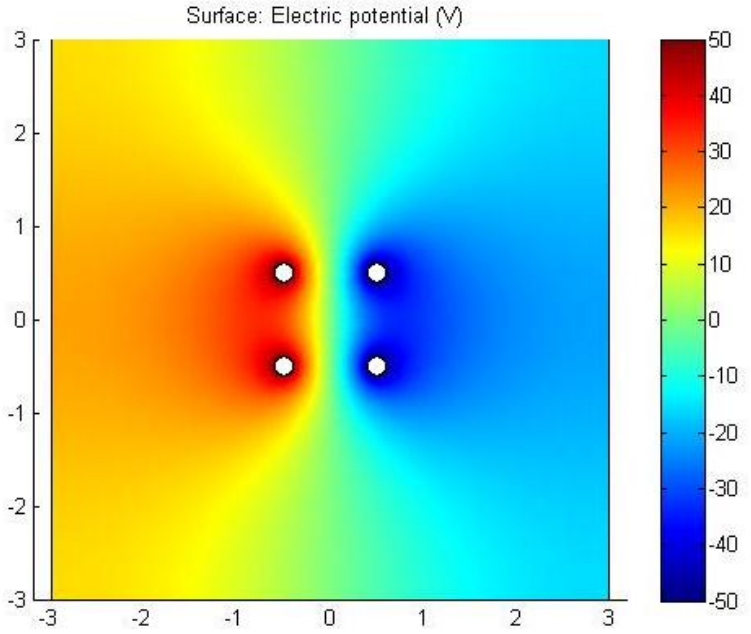

Figure 2.1: Bipolar electrode electric potential distribution for a bipolar RF catheter application on biological tissue

Bipolar electrodes are electrode pairs with dual polarity for current flow (Figure 2.1). It does not require the grounding pad that is needed for monopolar catheters. Bipolar electrodes can be arranged into electrode systems with 2 or more electrodes for large treatment area. Due to the close distance between electrodes, there is higher current density at the electrode-tissue interfaces and thus a higher and faster area of treatment in comparison to monopolar catheters. The Electric potential of the target tissue zone is govern by

$$\Delta \cdot E = \frac{\rho_c}{\varepsilon_0} \quad , \tag{2.1}$$

where ρ_c is the charge density, E is the electric potential and ε_0 the permittivity.

Bipolar catheters can be used for open surgery or to be integrated into laparoscopic devices (Chang 2011, Huang 2011). Haemmerich et al (2001) investigated the differences between monopolar and bipolar RF ablation with the use of a finite element model. It was concluded that the bipolar method creates larger lesions and is less dependent on local inhomogeneity in liver tissue.

Lim et al (2010) studied the effect of different Radiofrequency waveform on tumor ablation with blood vessel heat sink effect. RF waveforms such as half-sine, half-square, half-exponential and damped sine wave were simulated. It was concluded that the damped sine waveform creates the smallest RF lesion in volume while the half-sine wave form is the most effective.

RF ablation is most commonly used to destroy tumorous cells as a form of direct treatment. Tumors are subjected to cytotoxic temperature and results in cell necrosis. However, there are other usages for RF ablation in medicine. Liver resection, also known as hepatectomy, is the gold standard for liver tumor treatment. It is desirable to minimize blood losses during liver resection procedure for best treatment survivability. Dr Habib (Jiao 2006) pioneered a surgical procedure which uses RF ablation for hepatectomy. RF ablation was first performed on the desired line of resection to form a plane of coagulated tissue, followed by a manual resection with surgical scalpel. This reduces possible blood losses during resection and hence relieving usage of surgical maneuvers such as the Pringle maneuver (Milicevic 2008) which often results in results in ischemia-reperfusion hepatocellular injury. The technique can be performed by clinician whom is familiar with liver anatomy. The technique also results in reduction of the length of the anesthetic time

and the operating time as it is much faster to achieve coagulation in normal liver tissue compared to tumors.

Another usage for RF ablation is in the treatment for large tumors (3~8cm in diameter). Although Hepatectomy remains the gold standard for liver tumor treatment, only a low percentage of patients are eligible for the procedure (Tranberg 2004). RF ablation serves as a good alternative treatment for liver tumors due to its low invasiveness, simplicity and cost effectiveness (Ni 2005). Large tumor ablation is performed by overlapping zones of RF ablated tissue for full coverage of the tumor. In order to increase RF ablation area, many methods were developed such as saline injection (Livraghi 1997) for increased electrical conductivity, cooled electrodes to reduce charring (Goldberg 1996) and bipolar array to increase treatment zone area (McGahan 1996).

Radio-frequency ablation involves heat transfer in tissue which will be the main topic of discussion in this section. It is difficult to monitor actual temperature distribution in the tumor. Hence, it is suggested that modeling should be used for better understanding of the temperature distribution (Clegg 1993). Various works were done in modeling the RF ablation process with Penne's Bioheat Equation being the most commonly cited (Craciunescu 1998). While Penne's bioheat equation does not fully describe the full physical process of RF ablation, it is a good approximation especially for hyperthermia temperatures (Yang 2007). It is due to the temperature dependence of many different physical parameters such as dielectric and thermal properties which is crucial for simulation. Haemmerich (2001) suggested that Penne's assumption of heat transfer between tissue and blood occurs is not an accurate description. Nevertheless, the model describes blood perfusion with good accuracy if no large vessels are near the area of

concern. This limitation does not adversely affect the accuracy of Penne's model (Pennes 1948) in liver RF ablation as it is common to avoid the major vessel in the liver during surgery. It is also worth noting that variable such as conductivity; current density and blood perfusion do not change during ablation in Haemmerich's work and is assumed to be a constant in the model (6.4×10^{-3}). A modified Pennes bioheat equation for RF ablation simulation:

$$\rho c \frac{\partial T}{\partial t} = \nabla \cdot k \nabla T + J \cdot E - \rho_{bl} c_{bl} \omega_{bl} (T - T_{bl}), \tag{2.2}$$

where ρ is the density, c is the specific heat capacity of material, T is the temperature, k is the thermal conductivity, J is the current density, E is the electric potential, ρ_{bl} is the blood density, c_{bl} is the blood specific heat, ω_{bl} is the blood perfusion rate and T_{bl} is the blood temperature.

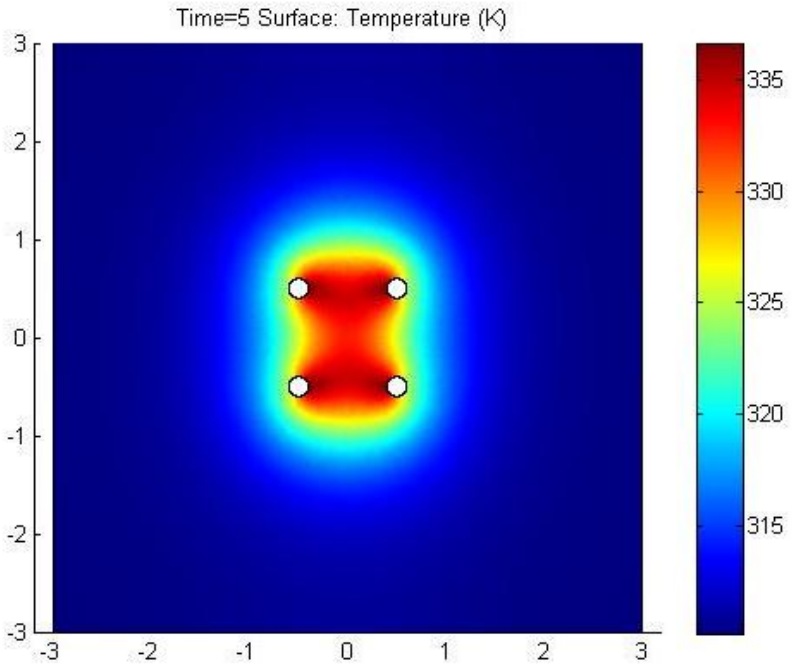

Figure 2.2. Finite element analysis of bi-polar RF ablation

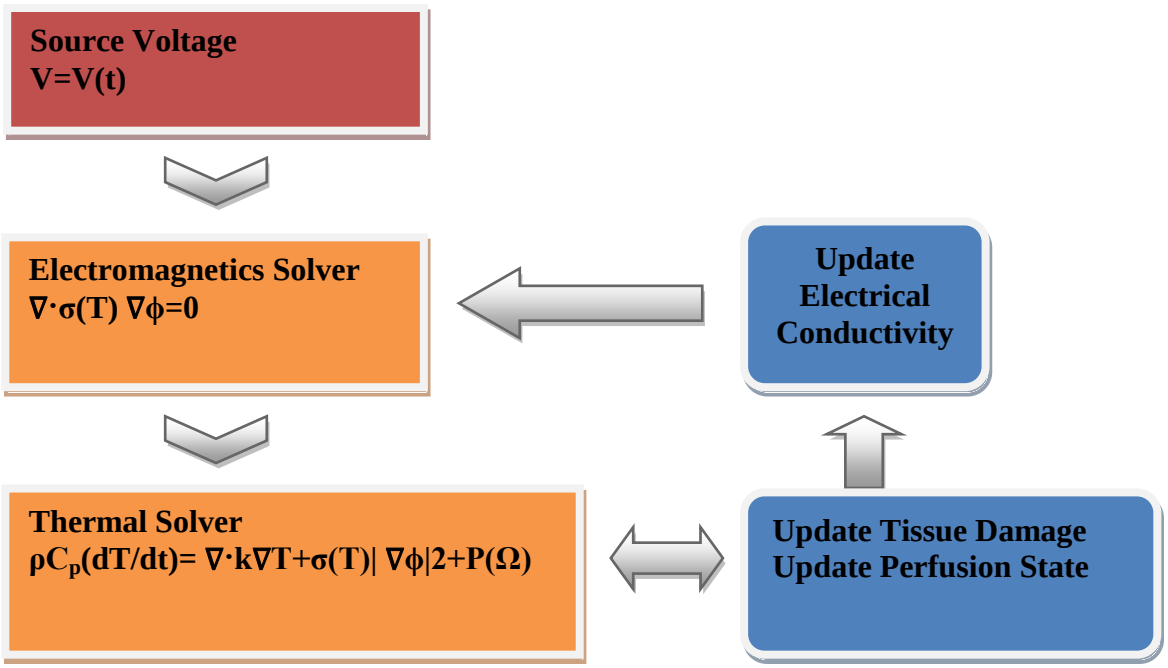

Figure 2.3. Illustration of Chang and Nguyen model (Chang 2004)

Finite Element (FE) method was used for simulation (Figure 2.2). The simulation incorporates the effect of Joule heating due to Electromagnetic energy which was not present in Penne's 1948 model. Chang and Nguyen attempted to model the radio frequency ablation process in soft tissue by means of a two dimensional finite element model (Chang 2004). The model takes into account both the temperature and electrical conductivity dependence of the RF ablation process with respect to the tissue. The results was compared to lesion sizes which involves iso-temperature contour as its definition and the study concluded that temperature isotherms may not be the best representation for actual tissue damage pattern. The model (Figure 2.3) has a close loop, self-updating structure consisting of the Specific Adsorption Rate (SAR) - the amount of energy absorbed by the tissue from the ablation needle, the Penne's bioheat equation for updating of tissue temperature, updating thermal conductivity of tissue and Arrhenius

equation to update the tissue damage and perfusion related. Tissue coagulation is assumed to occur when damage equation reaches a certain threshold (Ω=4.6) and that tissue coagulation is accompanied by the ceasing of perfusion. Once perfusion is stopped, the convective part of heat transfer due to perfusion is no longer valid, and the perfusion term is assumed to be zero.

Ahmed et al (2008) used an established computer simulation model of radiofrequency ablation to characterize the combined effects of varying perfusion, and electrical and thermal conductivity on RF heating. The varying electrical and thermal conductivities are used to represent tissue, fats and saline injection. The different parameters were changed to model the effect of RF heating in different scenarios. It was concluded that greatest RF heating occurred when the ablation needle surrounded by tissue and with an outer layer of fats. However, the model does not account for coagulation of blood vessels and thus the stopping of perfusion. Solazzo et al (2005) studied the effect of a varying background electrical conductivity to RF heating effectiveness. The team concluded that there is a strong relationship between background tissue and RF heating.

Bellia et al (2008) proposed the simulation of Penne's bioheat equation with transmission line method (TLM) and showed good agreement with other numerical methods. Roper (2004) used an integral transformation to formulate a benchmark solution for bioheat equation. Comparison of the benchmark solution with numerical solution shows close matches. Yang et al (2007) proposed a new bioheat equation for microwave ablation which includes tissue water evaporation, diffusion, vapor diffusion and

condensation due to the dominant of these physical processes when temperature reaches $100^{o}C$.

Arkin et al (1994) reviewed the different models proposed in modeling heat transfer in blood perfused tissue. The model aids in better predicting hyperthermia procedure which is relevant to the radiofrequency ablation technique we're studying. Due to the complex morphology of living tissues, hyperthermia modeling is often difficult and requires simplifying assumptions to be drawn. Penne's bioheat equation is inadequate in accounting for actual thermal equilibrium process between flowing blood and tissue. Penne's bioheat equation assumes that heat transfer occurs only through vessel walls and blood reaches tissue temperature immediately after entering the concerned vessel. Several techniques were reviewed for their strength and weaknesses. It was concluded that Pennes' model might still be the best practical approach. However, the main problem with bioheat transfer modeling remains the absence of measuring equipment capable of reliable evaluation of tissue properties and their variations at small scale. In addition, the model does not take into account denaturalization of the tissue causing structural changes and fluid exchanges when hyperthermia treatment is applied.

2.2 Mechanism of tissue injury

Tissue temperature is a direct cause of tissue injury which is quantifiable by cell death. All living cells are sensitive to temperature in certain degree. The result of thermal injury on different cellular structures and functions will ultimately determine whether the hyperthermia exposure results in reversible, partially reversibly or irreversible injury. Plasma Membrane is the first contact with cell by conductive heating. When membrane is

subjected to high temperature, it experiences phase changes into fluid form. Cytoskeleton is the structural proteins that form a filamentous network of microfilaments, microtubules and intermediate filaments. When subjected to hyperthermic treatments, the cytoskeleton loses its integrity and cells begin to round and fragment. The effects of hyperthermia on nuclear structure and function may have relevance to the viability of myocytes subjected to hyperthermia if marked nuclear disruption can be achieved in relevant temperature ranges.

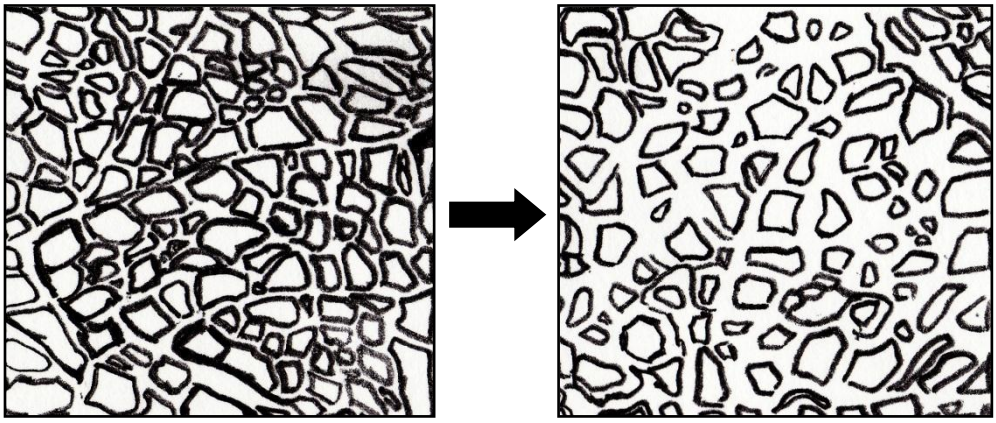

Figure 2.4: Changes in microstructure for tissue undergoing ablation. Increase in interstitial spacing and shrinkage in muscle fibre (Wierwille 2010)

Wierwille et al (2010) examined RF ablation lesions with optical coherence tomography and noted significant differences between ablated and non-ablated tissue. Shrinking of muscle fibers and an increase in interstitial area (Figure 2.4) was observed for tissue which underwent RF ablation. The ablated tissue has 31% less muscle to area ratio in relative. Larson et al (1996) examined the intraprostatic pathologic changes following accurately measured doses of transurethral microwave thermal energy in patients with benign prostatic hyperplasia. Pathologic findings were similar in all cases, consisting of sharply circumscribed intraprostate thermal injury with uniform

hemorrhagic necrosis and tissue devitalization without significant inflammation. Necrosis involved pure stromal nodules, mixed epithelial and stromal nodules, and predominately epithelial nodules. Mummified glands and stromal elements were noted in the areas of necrosis. Patchy acute and chronic inflammation was observed in the uninvolved prostate with a pattern suggesting mechanical disruption of the pathway for exit of secretions and consequent acinar rupture. Border between viable tissue and area of necrosis was sharply demarcated, extending no more than 1mm in thickness. This implied the tissue response to thermal energy was discrete rather than graduated. Thus, tissues exposed to a threshold thermal dose were devitalized, whereas tissues receiving lower thermal doses survived. Histopathologically demonstrable uniform thermoablation of a broad zone of obstructive prostate tissue can be achieved using an efficiently designed impedance matches transurethral microwave treatment catheter. Exposure of prostate tissue to temperatures higher than $45^{o}C$ for approximately 1 hour is sufficient for the ablation process.

The rate and magnitude of cellular damage increases with temperature and time which is well represented by an Arrhenius Equation. Membrane bleb formation in human fibroblast is observed when exposed to supraphysiologic temperature. During RF ablation, the high electric potential on the thin membrane (5-10 nm) gives a high electric field, resulting in membrane dielectric breakdown and electroporation. Animal cells cannot survive the temperature and times of the temperature related to structural protein denaturalization. Therefore, if pathologic examination of the acute lesions shows thermal damage zones of characteristic structural protein denaturation such as collagen swelling, hyalinization and birefringence loss, all cells in those zones will be dead.

Tumor cell necrosis occurs at 45^{o}C (Larson 1996) when held for long duration (hours) and within minutes when temperature is above 60^{o}C (Taton 2008, Baldwin 2001). Supraphysiologic temperature due to Joule heating during RF ablation causes cell membrane rupture near a threshold temperature (Lee 1991). A high relevance paper by Thomsen (2009) described the mechanism of cell and tissue death due to thermal injury. While the paper was written for thermal injury instead of thermal therapy, they share many common grounds. Cell death was defined as chemical and/or genetic phenomena and events that either signal the inevitability of death or appear at or close to the point of no recovery. Trivial as it may seem, cell death due to hyperthermia is not an easy classification due to the presence of apoptosis. Apoptosis is a programmed cellular death triggered by cell signals and is a constructive process for cellular renewal. Hence, more efforts would be required to quantify cell deaths due to heat induced injury or the naturally occurring apoptosis.

There are primary and secondary thermal mechanisms for thermally induced cell deaths. Primary mechanisms are due to higher temperature and within targeted heated volume. Several mechanisms of primary effects causing cell death are tissue mass ablation, tissue caramelization and carbonization, water evaporation, extracellular/intracellular stromal protein denaturalization and thermal dissociation. Secondary thermal mechanisms are related to other physical, chemical or biological processes which eventually lead to cell death via triggering apoptosis. The secondary thermal mechanisms are not related to heat but are responses from the living tissue when subjected to physiological ‘triggers’. Such ‘triggers’ include depletion of energy by stoppage of blood flow, production of reactive oxygen derived free radicals which causes

mitochondrial dysfunction, changes in membrane chemical influxes and concentrations and release of cytokines causing immune host responses.

Tissue injury or denaturalization results in a change in tissue modulus (Jiang 2007). Moffitt et al (2002) reported differences in mechanical properties between native liver and thermally damaged liver. It was concluded that the ultimate strength of native liver is higher than that of the thermally damaged liver. Walsh et al (1989) studied the effects of mechanical properties for guinea pig skin, bovine aorta, myocardium and liver on the efficiency of CO_2 laser ablation. It was concluded that ultimate tensile strength of tissue significantly affects the ablation efficiency.

Kiss et al (2004) investigated the viscoelastic properties of normal and thermally damaged canine liver tissue which underwent different temperature treatment. Mechanical tests were done and the results fitted to the classic Kevin-Voigt model and Kelvin-Voigt Fractional Derivative model. Kelvin-Vogit fractional Derivative model was concluded to exhibit better fit to experiment data. Obvious differences were observed between normal and thermally damaged tissue for the fit in the frequency domain, which exhibits viscoelastic properties. Jiang et al (2007) explained the potential of using ultrasonic elasticity imaging to monitor tissue coagulations in-vivo and proposed a biomechanical model to study deformation-based strain imaging due to RF ablation. Rupert (2009) monitored Radiofrequency lesion with an ultrasound scanner for elastography. The strain image was then compared to actual pathologically examined tissue lesions and it was concluded that area of lesion in the elastography slightly underestimates the actual region.

2.3 The role of bioimpedance in RF ablation

H.P Schwan of the University of Pennsylvania was among the first to experimentally measure the conductance and dielectric constant of soft tissues and cell suspensions over a broad frequency range (reference?). Many researchers (Raicu 1998, Whitathey 1982) in the field came up with different designs of probes for such dielectric property measurement in hope of reducing errors of measurement amounting from the electrode-tissue interface. Experimental work was also done on changes in dielectric properties of bovine liver at microwave frequency during heating (Chin 2000). Dielectric changes of kidney and fat were also studied when subjected to radio frequency thermal therapy (Dumas 2008). Both studies concluded that electrical properties do change after heating and hence makes our rationale behind modeling the heating process valid. Dumas made used of electrical impedance at 1kHz with a 4 electrode array as a predictor of quality of RF-induced lesions and proved that impedance is a good quantifying method for lesion completeness (O'Rourke 2007). Complete RF lesions increased resistivity by 21% inclusive of electrode-electrolyte interface currents and 30% without the interfacial currents. O'Rourke et al (2007) measured dielectric properties of human normal, malignant and cirrhotic liver tissue using an open-ended coaxial probe. The team concluded that dielectric properties of in vivo data cannot be represented in terms of a Cole-Cole model and hence further work is needed.

Esrick and McRae (1992) studied the effect of hyperthermia on the EMT6 tumor electrical conductivity and reported non-thermal conductivity related changes in the electrical conductivity. The study was to identify the problem related with the usage of Electrical Impedance Tomography (EIT) in tissue temperature measurement. The non-

thermal conductivity related changes are due to structural changes in the tissue due to hyperthermia. A method was devised to identify the onset of such structural changes in the tissue by comparing the slope of the impedance curve with the temperature curve between high frequency impedance (1MHz) and lower frequency impedance (44KHz). It was concluded that the devised impedance method only determines temperature changes and not the actual tissue temperatures.

In another work by Esrick and McRae (1992), electrical impedance from 100Hz to 40 MHz of freshly excised EMT-6 tumors was measured when exposed to heat. The tumor response sequence includes cellular swelling, progressive membrane damage, cellular shrinking and progressive histolysis (dissolution of tissue). The A software (STEPIT) was employed to fit experimental data to the Cole-Cole model and it was concluded that the Cole-Cole parameter α increased during the histological changes. Fitting shows that parameters such as characteristic frequency, dielectric constant and conductivity all exhibit changes related to the swelling of cells to a maximum and then contraction. It was found that tissue when excised exhibit small change in dielectric properties for temperature above 31^{o}C, apparently due to ischemia.

Gersing (1999) investigated the electrical conductivity in living tissue when subjected to heating to the temperature of 42.5^{o}C (Figure 2.5). Tumor (DS sacorma) and skeletal muscles of rats undergoing heat treatment were studied. Experiments were done to study the effects of fluid volume shift in the tissue when subjected to heating for both high frequency and low frequency conductance. An impedance analyzer was used to measure the changes in conductance due to heating from an infrared source. The conductance values for both high frequency and low frequency was plotted with time. A

temperature coefficient corrected plot with an assumed temperature coefficient (1.5~2.5%/^{o}C) was also included. The tissue thermal conductivity was also taken into consideration and was concluded that the changes in conductance measured during hyperthermic treatment were not exclusively due to temperature coefficient but also a change in extracellular and total fluid content. It was also concluded that a permanent change in structure is obtained after heating is stopped and tissue is allowed to return to its original temperature.

Ko et al (2001) measured the effect of bioimpedance on radiofrequency catheter ablation in 55 patients undergoing AV nodal reentrant tachycardia (AVNRT). The measured bioimpedance was correlated to the efficiency of heating (ratio of average temperature to average power). It was found that preablation bioimpedance have positive correlation with maximal temperature, average temperature and the efficiency of heating. Negative correlation was found between preablation bioimpedance and average power. Catheter contact pressure, catheter tip orientation and convective cooling by blood flow also proved to affect efficiency of ablation. This conclusion aids in the development of modeling the ablation process and a further confirmation that impedance is a good property to model RF

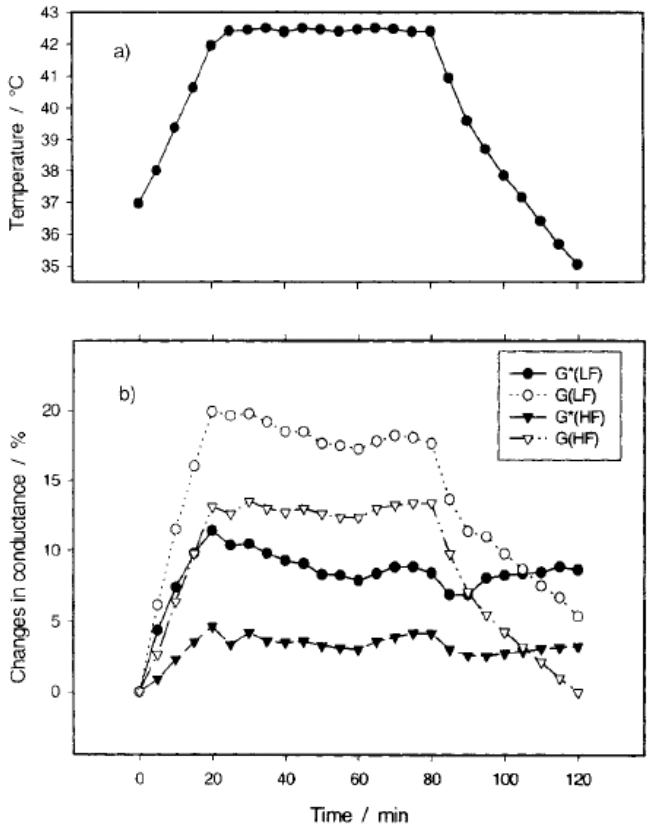

Figure 2.5. Plot of conductance changes with time. (Gersing 1999)

2.4 Blood flow modeling

Hoetink et al (2004) developed a theory to explain the laminar flow dependency of low frequency conductivity of blood in a rigid cylindrical tube (Poiseuille flow). Assumption was made that blood is a Newtonian fluid and that red blood cells are represented by ellipsoidal particles. Red blood cells were assumed to be surrounded by plasma and form a control volume which is small in relative to tube size. The theory is built upon the Maxwell-Fricke equation which assumes conductivity of Red Blood Cell to be negligible compared to plasma conductivity and is a function of hematocrit and orientation of the cells. Hoetink (2004) studied work by Evans on the deformation of Red

blood cell due to fluid flow and derived it as a function of shear stress from the conservation of volume. Shear stress profile of a fully developed stationary laminar flow in Poiseuille flow was also adapted to relate it to the reduced average velocity of the blood flow. Experimental work was done to verify the validity of the model and it proves to be more reliable than Maxwell-Fricke equation which does not take into account deformation of red blood cells due to fluid flow. This result bolster the approach of using impedance for quantitative assessment of blood flow as flow velocity does affect the impedance measurement of the sample.

Sakamoto et al (1999) noticed the lack of measurement for fluid shifts during hemodialysis which causes symptoms in patients (headaches, nausea, etc.). A model was built for erythrocyte (red blood cell) orientation and deformation and their effect on blood impedance. They observed from experiments that the size and shape of erythrocyte changes with osmotic pressure and hence increases in size when osmotic pressure of plasma is changed. The erythrocyte is represented by a geometrical model with an equivalent permittivity of:

$$\varepsilon_{\alpha}^{*} = \frac{2\varepsilon_{M}^{*}+(\varepsilon^{*}-\varepsilon_{M}^{*})a_1b_1c_1\left[\int_0^{\sigma}\frac{d\lambda}{(\lambda+\alpha_1^2)R_1(\lambda)}+\frac{2}{a_2b_2c_2}\right]}{2\varepsilon_{M}^{*}+(\varepsilon^{*}-\varepsilon_{M}^{*})a_1b_1c_1\int_0^{\sigma}\frac{d\lambda}{(\lambda+\alpha_1^2)R_1(\lambda)}}\varepsilon_{M}^{*}\,, \qquad (2.3)$$

where $R_1(\lambda) = \{(\lambda + a_1^2)(\lambda + b_1^2)(\lambda + c_1^2)\}^{1/2}$.

Constants $a1, b1, c1, a2, b2\ and\ c2$ represents the length of the axis for the memberane interior and exterior ellipsoid.λ represents the pressure, ε* represents the interior permittivity of the erythorocyte and ε^*_M represents the membrance permittivity. The author represented the flowing blood in an equivalent circuit similar in structure to that of the Debye model (Figure 2.6 & 2.7).

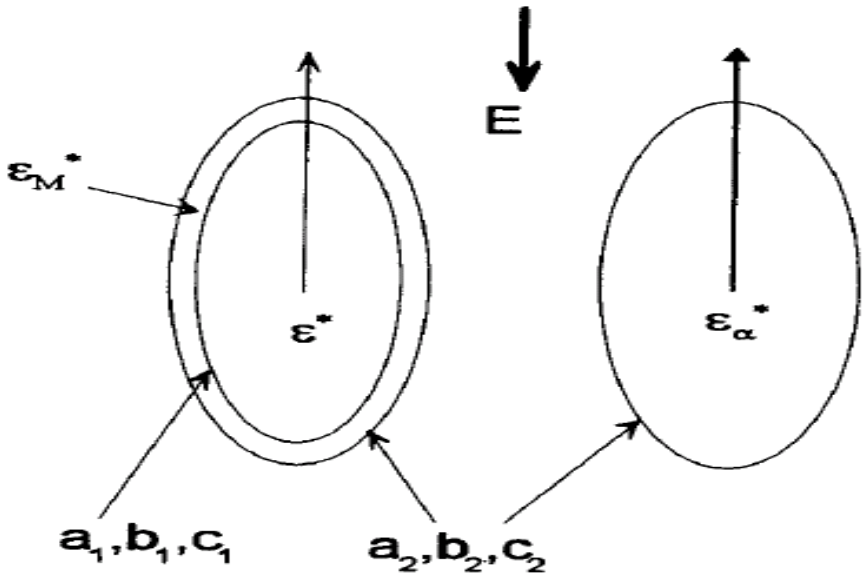

Figure 2.6. Sakamoto's model of dielectric of red blood cell (Sakamoto 1999)

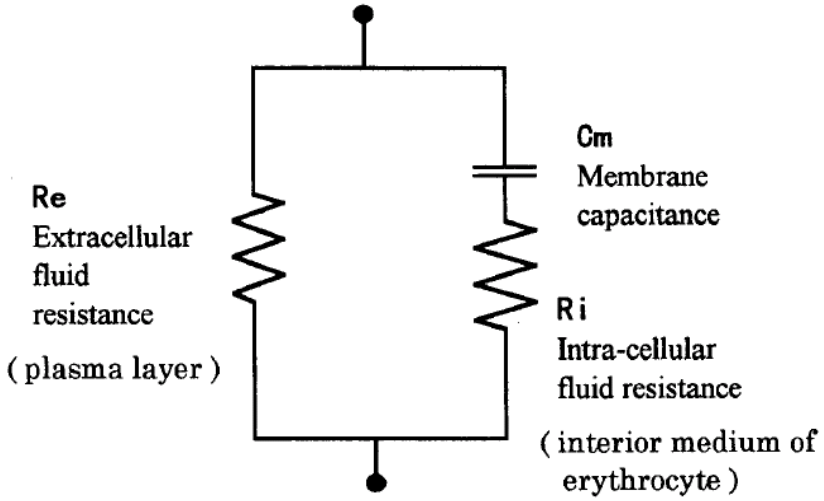

Figure 2.7. Equivalent circuit for flowing blood (Sakamoto 1999)

The erythrocyte interior consists of hemoglobin and saline which is assumed to be a spherical electrical insulator in a suspension. An equivalent circuit for the erythrocyte is proposed to be of the structure below, and we will be adopting this model for our future model for blood flow.

Jaffrin et al (1997) investigated a technique to monitor extra and intracellular volume during hemodialysis. It was known that the extracellular resistance is represented by the low frequency resistance while the high frequency resistance represents both the intracellular and extracellular resistance. From experimental results, it was concluded that Fricke's classic model is not suitable for tissue and blood due to the many form of cell types. Cole-Cole model is more suitable for fitting the experimental results of the sample. The high and low frequency for monitoring the resistance is 5 kHz and 1000 kHz respectively. The resistance for extracellular volume, represented by resistance at low frequency is:

$$R_e = \frac{\rho_e l^2}{k_e(V_{e0} - V_{UF})} \cong \frac{\rho_e l^2}{k_e V_{e0}} \left(1 + \frac{V_{UF}}{V_{e0}}\right) , \tag{2.4}$$

the resistance of the model at high frequency is represented by:

$$R_\infty \cong \left(1 + \frac{k_e V_{UF}}{\rho_e l^2 A}\right) \frac{l^2}{\frac{k_i V_{i0}}{\rho_i} + \frac{k_e V_{e0}}{\rho_e}} \quad , \tag{2.5}$$

where ρ_e is the resistivity of the extracellular matrix, ρ_i is the resistivity of the intracellular matrix, k_e is the shape factor for extracellular matrix, k_i is the shape factor for intracellular matrix, V_{e0} is the initial volume of the extracellular matrix, V_{i0} is the initial volume of the intracellular matrix and V_{UF} is the ultra-filtered volume.

Liu et al (1999) obtained a closed form solution of Pennes' bioheat equation when skin is subjected to heat flux. Two modes of heat flux is employed, a constant heat flux and a sinusoidal heat flux. The close form solution suggested that there will be an observable phase shift in temperature response which is related to the average blood perfusion under the skin. The effect of blood perfusion on phase shift is inversely dependent on the heating frequency. The sensitivity of the solution is also dependent on

frequency, and it is desirable to choose a lower frequency of heating for less sensitivity to error and higher impact due to blood perfusion. Thermal contact resistance is a major source of error in the model but can be eliminated by usage of conducting grease. In addition to the possible error, RFA makes use of thermal energy to cause tissue denaturalization hence could be a source of disturbance to this heat flux method.

2.5 Multi-scale modeling

Multi-scale modeling is an upcoming technique for modeling and is very much applicable to biological tissue due to its inherent hierarchical structure. A definition of multi-scale model is a model which includes components from two or more of these levels of organization (multiple length scales). One of the main aims of multi-scale model is to couple all complex levels of biology together to produce integrated model across multiple spatial scales and physical processes. As even more complex models are developed, it will be necessary to develop new methods to model the different levels, in particular in coupling across the interface between stochastic and deterministic processes and new techniques will be required to compute their solutions efficiently on massively parallel computers. Chui et al. (2002) proposed integrating a multi-level biomechanical model into an integrated medical simulation system. The model is focused on the liver organ which is the largest organ in size and the major chemical factory within the human body. The work is relevant to the approach of a multi-scale model bioimpedance model which will be covered in later sections.

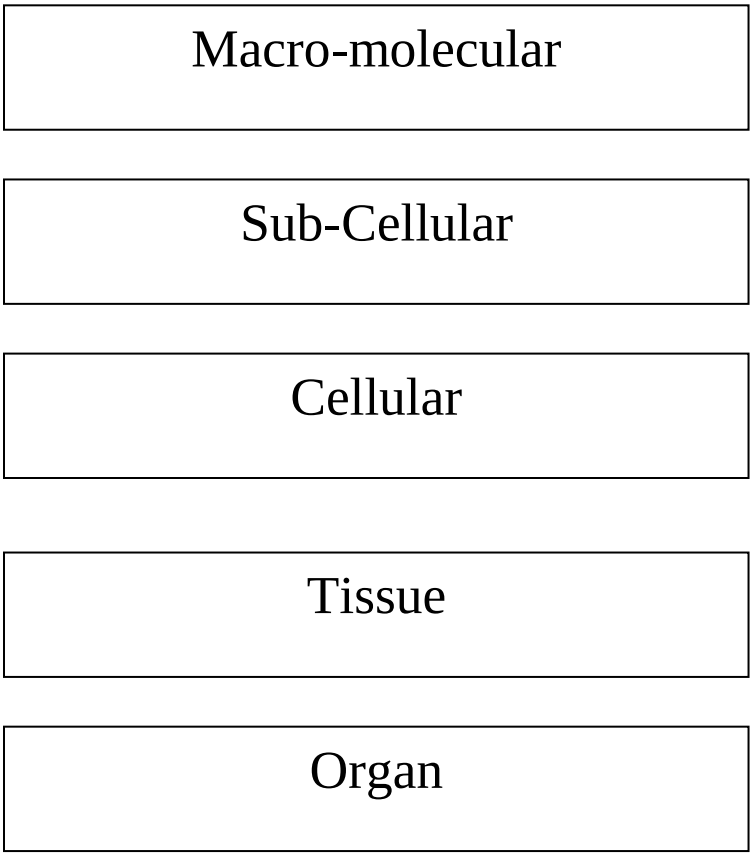

Figure 2.8. Different levels of biological structure.

Described in this section are the various levels of organization (Figure 2.8) :

Macro-molecular – Groups of particle as single entity. At molecular level, Newton's laws govern behavior of the system and modeling process amounts to determination of an appropriate force field to describe the interaction between particles.

Sub-cellular (Mesoscopic scale) – When number of particles present in system becomes sufficiently large, it becomes possible to treat system as a single continuum. Allows flux of various substances to be modeled by processes such as diffusion or convection, which can be modeled using partial differential equations (PDEs) and spatially varying density

functions rather than having to keep track of individual particles (or groups of particles). Upper bound of this single continuum level is whole cell.

Cellular – Basic structural and functional unit of an organism is the cell. Typical size of a cell is ~10^{-5}, with great variety amongst different types. Cellular level is a natural starting point for many integrative physiological models: cells are small enough to encapsulate many microscopic processes, yet large enough to influence macroscopic behavior. Many of the interactions of a cell with other cells and the extra-cellular space can be summarized by recoding the flux of various substances (ions, nutrients) across the cell membrane- suggesting formulation of conservation laws in the form of ordinary differential equations (ODEs) to describe them, providing a natural way of modeling their behavior.

Tissue – Tissue level is a large group of connected cells of the same type performing a specific function. In addition to cells, a region of tissue will typically contain an extra-cellular matrix (ECM) that holds the cells together and gives them structural stability. Mechanical models are usually formulated at tissue level. Model usually consists of partial differential equations (PDEs) (or sometimes cellular automata) rather than ODEs generally seen at cellular level. Amount of time required to run simulation varies, but generally solved relatively quick if there is no interaction with models at cell level.

Organ – Discrete unit performing a function or group of functions. At organ level, modeling usually consists of integrating tissue level models with one another and with a

representation of the geometry of the organ that is being modeled. Tissue level models can be computationally demanding. Tissue models embedded within require even longer simulating.

The main difficulty in multi-scale modeling is to develop a link or a way to couple the different size scale. We applied multi-length-scale modeling to model the impedance of liver tissue. Other form of multi-scale model such as multi-time-scale and multi-physics-scale are not relevant in our context.

When models are coupled together in this way, the number of variables becomes very large. The system of governing equations is now a large system modeling multi-scale processes. Equations representing multi-scale processes are stiff (Southern 2008). As a rule of thumb it is usually much more efficient to use implicit numerical methods to solve stiff problems. Alternatively, in some cases, rather than combining the two models explicitly as described above, it may be possible to use the results of one model as input to the second. Sometimes it may also be possible to formulate boundary or initial conditions for a model on a larger spatial or time scale in terms of the results of another model at a smaller scale.

Burrage et al (2004) have reviewed some of the possible methods for incorporating stochastic processes in a deterministic framework (in particular the formulation of stochastic differential equations) in the context of chemical reactions that occur on multiple time scales. However, this has not been applied to any large-scale problem in the life sciences and has great potential in biological modeling.

2.6 Stochastic finite element method

Stochastic Finite Element (SFE) method is the combination of statistical methods with deterministic physical models to account for variation and noise in simulation. The method relies on a statistical probability density distribution for parameter values which mimics the inherent biological tissue structural variations. Stefanou et al (2009) discusses the various frameworks of SFE method in the field of analysis of uncertain systems in which uncertainty often occurs to the inputs of the system. Although most inputs are non-Gaussian in nature, many works has inputs often described to be statistically Gaussian. The Gaussian assumption is simple and convenient due to the lack of experimental data. In addition, the Gaussian random fields are naturally occurring due to Central limit theorem.

While the method was mainly used in structural engineering (Beck 2006, Argyris 2002, Baroth 2006, Kiureghian 1988), the method is slowly finding its way into biomedical applications. Fuentes (2012) used SFE method in a stochastic form of Penne's Bioheat equation integrated with a Kalman filter to provide temperature field estimates in time of data loss. Clinical data was collected with the use of Magnetic Resonance Temperature Imaging (MRTI) with partial temperature information removed. The residue data act as a reference to the Kalman filter and results simulated shows accuracy with no effect of Kalman filter on known data points.

Hu (2010) studied the behavior of the human placenta tissue on impact, which is the highest cause of fetal death in accidents, with stochastic finite element analysis of a visco-hyperelastic model. Material of statistical nature was used with results showing good agreement with actual data and simulated results. Gao (1997) employed stochastic

finite element analysis to simulate noise and scattering present in time-resolved optical tomography imaging. Photon propagation scattering and noise from measuring device both contributed to variations in data and hence uncertainty. The method allows a forward problem simulation for verification of their proposed inverse problem solving utilizing Tikhonov-Miller regularization method.

Delalleau et al (2011) investigated the usage of stochastic method in solving inverse optimizing problem. Elastic properties of skin were modeled by two models: a classic single layer hyperelastic model and a double layer neo-Hookean potential model. The purpose of the study was to observe the performance of such stochastic optimization method and concluded that there is potential in the novel approach.

Chapter 3

MULTISCALE MODEL FOR BIOIMPEDANCE MODELING

Huang WH, Chui CK, Teoh SH, Chang SK, 2012. A multiscale model for bioimpedance dispersion of liver tissue. IEEE Trans Biomed Eng, 59(6),1593-7.

This chapter contains work from the above cited journal paper which was published in 2012. The chapter introduces a multi-scale bioimpedance model to model bioimpedance dispersion of the hepatic tissue. Section 1 gives an overview on multi-scale modeling and section 2 presents the existing work in bioimpedance modeling. Section 3

covers the new multi-scale bioimpedance model with the following section presenting the simulation and results in comparison with classical models. The last section discusses the presented work.

3.1 Multi-scale modeling

Multi-scale modeling is particularly applicable to biological tissue modeling due to the inherent hierarchical structure of biological tissue. One of the main aims of multi-scale modeling is to couple all complex levels of biology together to produce integrated model across multiple spatial scales. Chui (2002) proposed integrating a multi-level biomechanical model into an integrated medical simulation system. The model focused on the liver organ which is the largest organ in size and the major chemical factory within

the human body. In section 2.3, the role of bioimpedance in RF ablation treatment is well reviewed. Bioimpedance plays an important role in the effectiveness of RF ablation due to the energy deposition dependency on tissue electrical conductivity. Section 2.4 reviews how blood flow in tissue affects bioimpedance. This enables bioimpedance to be used for blood sensing technology due to the shift in bioimpedance in the presence of blood. A better understanding of bioimpedance is useful in providing a more accurate RF ablation simulation as well as an insight into tissue structure, composition and blood content.

In this chapter, multi-length-scale modeling is applied for modeling the bioimpedance of liver tissue. The model is built on the basis of a self-similar structure with sound physiological reasoning, and includes the many hierarchical levels of the liver tissue. The model also includes the existence of blood vessels for each scale which accounts for blood content in the tissue. The model is able to mimic experimental data of actual liver tissue bioimpedance dispersion more accurately than the highly cited classic Cole-Cole model.

When models of different scales are coupled together, the number of variables becomes very large. The governing equations are built from a multi-scale process which results in a large system model. In the model, no stochastic terms were incorporated due to the self-similar structure of liver tissue and to reduce complexity.

3.2 Bioimpedance modeling

Bioimpedance is the electrical property of the biological material when subjected to an electric field of different frequency. Bioimpedance has been a widely studied topic since early 20th century, with many related medical technologies such as Electrocardiography (ECG) which is the interpretation of electrical activity of the heart in the time frame and bioimpedance plethysmography which is the measurement of pulsatile blood volume changes in the aorta. Electrical properties of biological tissue exhibits an unusual response in the frequency domain which was later defined as the α, β and γ dispersion (Schwan 1999, Figure 3.1). It was mentioned that β dispersion (low frequency) and γ dispersion (high frequency) exhibits different tissue values. β dispersion value indicates extracellular content and gamma dispersion values exhibits total electrolyte content. If impedance values of these two frequencies are collected, it is thus possible to plot the changes in impedance hence inferring the changes in tissue structure when tissue is undergoing ablation. An inverse can also be done, by observing histological changes; the impedance of the tissue can then be predicted.

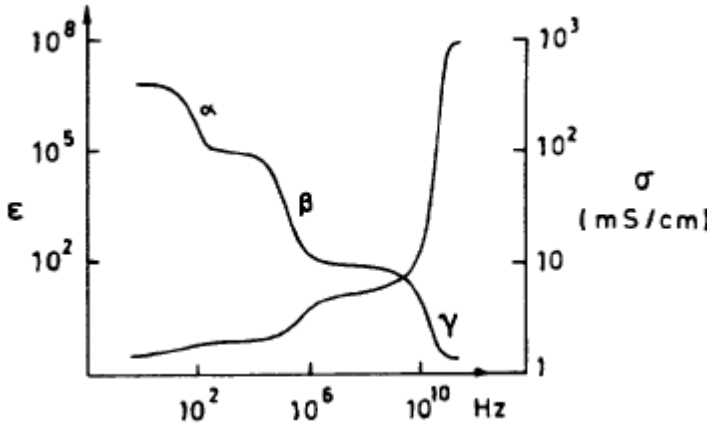

Alpha Dispersion – 10 Hz to 1 KHz – Associated with ionic diffusion processes at site of cellular membrane

Beta Dispersion – 100 KHz to 10 MHz – Polarization of cellular membranes which act as barriers to flow of ions between intra and extra cellular media

Gamma Dispersion – Above 1 GHz - Polarization of water molecules

Figure 3.1. Bioimpedance dispersion (Schwan 1999)

Many models were explored regarding dielectric properties of soft tissue in its frequency domain since the 1940s. Most of the models explored relate the dielectric property of soft tissue in the frequency domain. It is evident that such an approach is necessary as impedance of soft tissue is frequency dependent and should be modeled based on the frequency of the input signal. The famous Cole-Cole model (Cole 1941) is an empirical model which has several relaxation time constants in the frequency domain pertaining to the relaxation of dielectric materials commonly encountered in experiments. Cole compared the classical dielectric model which is the Debye model (Figure 3.2) to experimental results and concluded a discrepancy between them. The Debye model does not fit well with the impedance readings from experimental results for both liquid and solid materials. Cole proposed a new empirical formula which is a general form of the Debye model with a parameter α which ranges between 0 and 1. This parameter depresses the semicircular plot of the Debye model on the complex plane and leads better fit when compared to experimental data. The model results in an equivalent circuit with a constant phase element of phase 1/2απ. This is the same as the angle made by the radius vector to ε_∞, and hence material satisfying such locus can be quantified by α. However, there is no physical interpretation behind the constant phase element. The Debye model can be described by Equation 3.1

$$\varepsilon^* - \varepsilon_\infty = \frac{(\varepsilon_0 - \varepsilon_\infty)}{1 + i\omega\tau_0} \tag{3.1}$$

in comparison to Cole-Cole model described in Equation 3.2

$$\varepsilon^* - \varepsilon_\infty = \frac{(\varepsilon_0 - \varepsilon_\infty)}{[1 + (i\omega\tau_0)^{1-\alpha}]} \tag{3.2}.$$

The Cole-Cole model is widely used in the field of bioimpedance. There is however a lack of theoretical explanation behind the formulation of the Cole-Cole model. No physical explanation behind the presence of the constant phase angle element. It is the motivation of this proposal to propose a model that can fit the Cole-Cole model yet has a sound physical explanation.

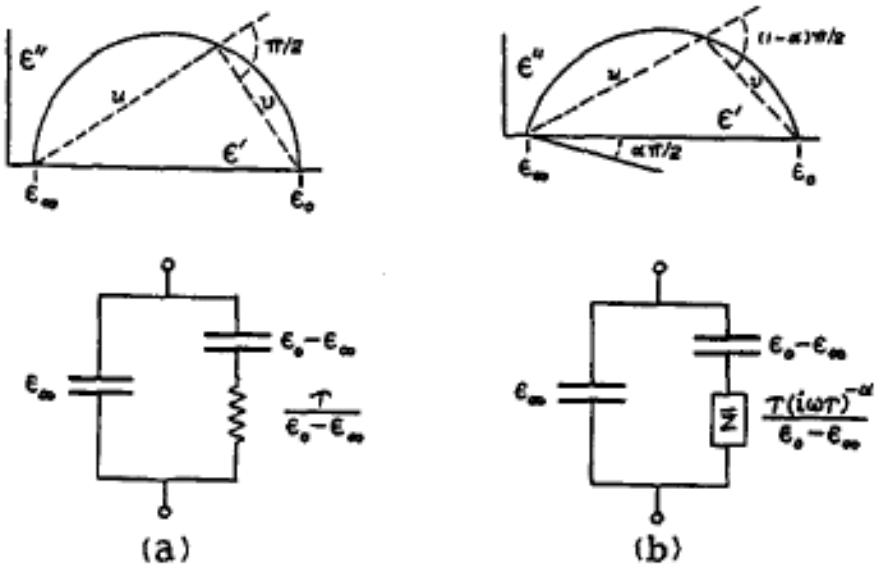

Debye Model Cole-Cole Model

Figure 3.2. Comparison between Debye and Cole-Cole model (Cole 1941)

There were several critics of the Cole-Cole model. Lazebnik (2006) concluded that the dielectric properties are temperature dependent and thus inadequacy of the Cole-Cole model. Grimnes (2005) concluded that an alternative model with conductance as free parameter will be a better representation. Authors Grimnes and Martinsen reviewed the famous Cole Impedance model, its restrictions and proposed an alternative model. Cole model is a modified Debye model by replacing the constant capacitor with a general constant phase element. The constant phase elements results in a depressed circle which

is often observed in experimental data related to impedance for tissue and cell suspensions. However, the limitation of the Debye model is that the time constant of the model is conductance independent and hence incompatible with general relaxation theory. The alternative model proposed does not have such incompatibility issue. However, it has 5 parameters instead of 4 from the Cole Model and is not a straight forward curve fit unlike the Cole model. Although faced with much limitation, the Cole-Cole model is still the most frequently cited model and is often used as a comparison for Bioimpedance models.

Different approaches have been proposed to address the problem of modeling the dispersion relationship of soft tissue theoretically. Hanai et al. (1960) described tissue as a concentrated suspension of weakly conducting spheres in a conducting medium with each sphere experiencing a uniform mean field. Chiew and Glandt (1984) described the effect of structure in a hard sphere model of a material on effective conductivity. Kunii (1998) modeled liver tissue in a simplified electrical model geometrically, assuming the cell to be of circular shape and contains nucleus and organelles to be of circular shape. Yasuno et al. (2006) modeled biological tissue in an equivalent circuit model for local EIT by arranging the equivalent model in cross networks of resistor and capacitor. Kunii et al (1998) made used of a lumped element circuit model with an increasing branch of resistor and capacitor in series in modeling of soft tissue of different sizes. Smye (2007) adopted the dielectric model for porous media suggested by Hilfer (1990) and applied it for modeling of electrical properties of tissue. Making use of porosity theories and percolation theory, the model intakes histological data from high definition images and incorporates them into the dielectric model thus overcoming the conventional restriction

of modeling cells as circular in a medium. However, this approach lacks geometrical accuracy and hence limits its usefulness.

Smye's model (Smye 2001) can be described by

$$\frac{2\Delta}{3\varepsilon} = \int_{\emptyset_p}^{\emptyset_0} \frac{X^* + \emptyset Y^*}{E(\emptyset)} d\emptyset + \int_{\emptyset_0}^{\emptyset_p} \frac{\varepsilon_{ecf} + \emptyset Y}{\varepsilon_{ecf} X - 2\varepsilon \emptyset Y} d\emptyset$$

where

$$X = a + ib + 2\varepsilon, Y = c - a + i(h - b), E(\emptyset) = XX^* + (Y^*X + X^*Y)\emptyset + YY^*$$

$$a = \frac{\{c(1+\eta c)+\eta h^2\}}{\{(1+\eta c)^2+\eta^2 h^2\}}, b = \frac{h}{\{(1+\eta c)^2+\eta^2 h^2\}}, c = Re(\varepsilon_{ecf}), h = \frac{\sigma_{ecf}}{2\pi f \varepsilon_0}, \eta = \frac{2\varepsilon_0}{C_m t} \qquad (3.3).$$

The model assumed that unit cells are in random and spaces between cells are occupied by conducting medium (extracellular medium). A probability density function is used to represent the probability of finding the local porosity within a range at any given point in the volume. The tissue is assumed to be homogeneous; hence the probability density function is independent of position. Effective medium theory was used to find the local effective complex permittivity by solving the integral of conductivity and capacitance of the sample. Lastly, an equation is derived for the permittivity of the tissue sample as a function of two integrals of porosity. Various parameters were varied in the model and shows similar response to that of the Cole-Cole model which is used as a benchmark for model verification.

Walker et al (2000) did work on modeling the electrical impedance of normal and premalignant cervical tissue by using finite element analysis and modeling them according to histological differences between the tissue structures for each phase and concluded that tissue structure affects the impedance results.

Dissado (1995) proposed a dielectric response model based on a fractal interpretation of the power law behavior observed during experiments. The interpretation allows the response to be related to the different scale of sub-cellular and cellular organization of the tissue. Dissado proposes two responses namely the constant phase angle response and the quasi-DC response to account for the dispersion in soft tissue. The constant phase angle response is a deterministic model in which tubular hierarchy is reproduced in the other sub levels and can be analyzed by a fractional power law. The constant phase angle response is used to model blood vessels and ducts which have tubular branched structure. This approach will be similar to the one we are proposing which is related to the structural organization of the liver tissue. The Quasi-DC response is a hierarchical model built on an equivalent circuit (Figure 3.3) which is self-similar. The response was proposed to account for conductivity due to extracellular medium in the tissue. This model can be described in terms of a percolation cluster which is a stochastic fractal model. This aids in accounting for variation in tissue structure.

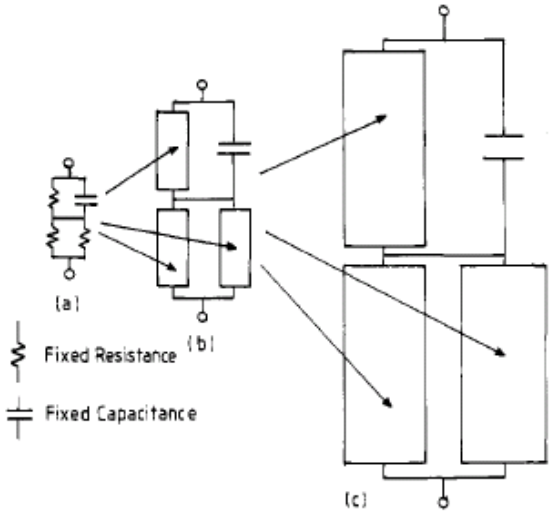

Figure 3.3. Hierarchical model (Dissado 1905)

H.P Schwan (1980) discussed the relation between temperature and dielectric properties of biological systems and concluded that the dielectric properties change by 2% for every unit change in temperature. He went on to explain the various mechanisms behind the temperature dependency of the dielectric properties for the various dispersion phases. However, the model does not account for coagulation and moisture lost due to Joule heating hence implying the inadequacy of modeling RF ablation by temperature alone without considering structural changes.

The above models are not feasible for our application as they do not differentiate between blood vessels and extra-cellular medium. Indifference in the two would result in inability of the model to determine the changes in impedance due to variation in blood flow and extracellular matrix independently.

3.3 Multi-scale bioimpedance model

Presented in this section is a new multi-scale liver bioimpedance model (Figure 3.4) exhibits impedance response in frequency domain and is able to account for various bioimpedance dispersions. The model might be the first multi-scale model to our knowledge which is able to include the β and γ dispersions in a single model that varies with frequency. Current models, such as the Debye model or Cole-Cole model are only capable of representing dispersions individually. Two Cole-Cole models will be required to represent the β and γ dispersion respectively.

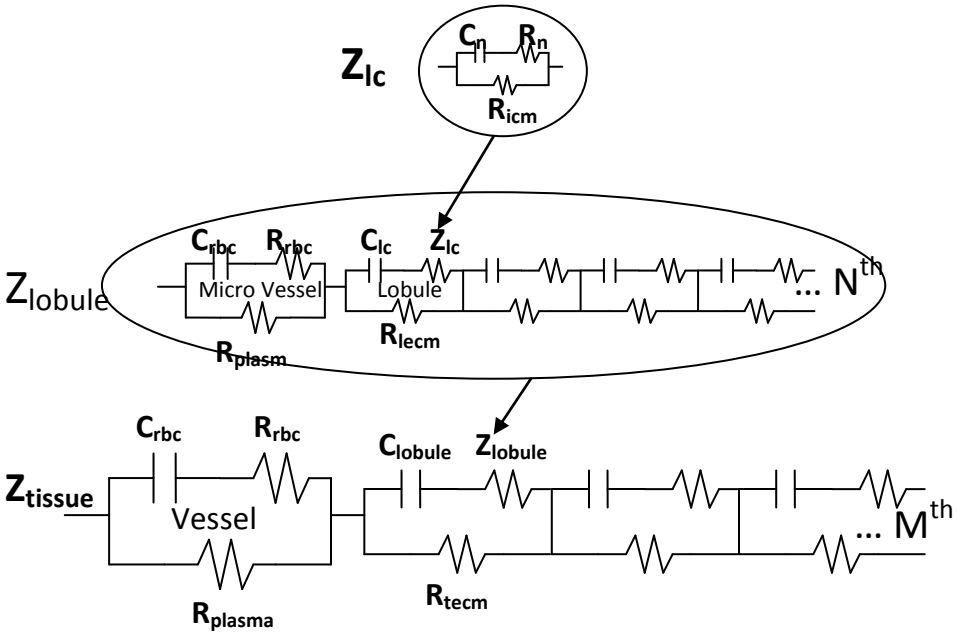

Figure 3.4. Proposed multi-scale impedance model

The new model consists of self-similar equivalent circuit comprising resistors and capacitors. Each individual repeating unit of blood, liver cells, liver lobules and liver tissue is assumed to be identical to each other and to share the same parametric value. This assumption applies to the structure in other levels; lobule and tissue level and is deterministic in nature. Although the variation among the similar units which is present in actual physiology is not considered, the parameters in the model represent the mean value for the unit and its combined impedance response. The model also assumes a constant hematocrit (ratio of blood occupied by red blood cells) for all blood present in the model. Homogeneity in such models is often implicitly assumed in existing literature (Yasuno 2006, Kunii 1998, Syme 2007, Dissado 1995) and is validated with experimental data.

The fundamental unit of the model, which is the hepatocyte, or liver cell, is represented by a Debye model and has a complex resistivity value of Z_{lc}. The Debye model consists of a resistor in parallel to a branch which contains a capacitor and a resistor in series. The capacitor C_n represents the liver cell nucleus membrane; the resistor R_n represents the resistance of the cell nucleus matrix while the resistor R_{icm} represents the intracellular matrix which surrounds the cell. The cell membrane acts as an open circuit at DC/low frequency, allowing electrical current to flow through the extracellular matrix surrounding the cell (Figure 3.5). The complex resistivity of the cell is largely resistive at low frequency. However, as the frequency increases, the complex resistivity becomes increasingly capacitive and at high frequency, the complex resistivity value is equal to the two resistors R_n and R_{ecm} in parallel. This is an actual physical process often related to the dispersion behavior of bioimpedance and is the basis of our multi-scale model. The liver cell can be represented by the equation:

$$Z_{lc} = \frac{R_{icm}+i\omega_{icm}R_nC_n}{1+i\omega C_n(R_{icm}+R_n)}\,, \tag{3.4}$$

where R_{icm} is the resistance of intracellular matrix, R_n is the resistance of nucleus interior and C_n is the capacitance of nucleus membrane.

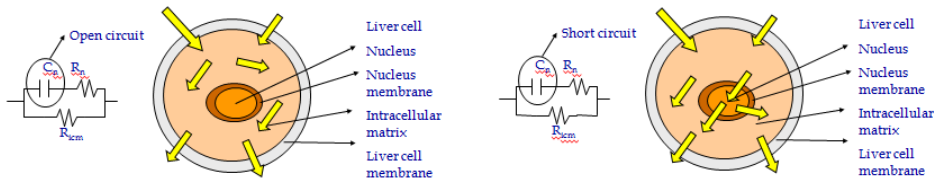

Figure 3.5. Liver cell model. (left) low frequency behavior of liver cell (right) high frequency behavior of liver cell.

The next level in the model is the liver lobule level. The liver lobule consists of many liver cells and a central vein which is consistent in all liver lobules. The central

vein is represented by a structure similar to that of the liver cell but with a different value for the complex resistivity. The liver cells modeled above are integrated into the lobule level with variable *N* relative volume of liver cells. The liver cells are in series with the central vein forming the liver lobule equivalent circuit. The structure can be explained physically as follows.

When a current at low frequency passes through the liver lobule, the path of the lowest resistance will be taken (Figure 3.6). This path consists of the extracellular matrix and the plasma in the blood. At high frequency, the current passes through the membrane and into the vessels as well as the liver cells. Complex resistance due to the central vein is:

$$Z_{mv} = LZ_{blood} = L\frac{R_{plasma}+i\omega R_{plasma}R_{rbc}C_{rbc}}{1+i\omega C_{rbc}(R_{plasma}+R_{rbc})}, \tag{3.5}$$

where R_{plasma} is the resistance of blood plasma, R_{rbc} is the resistance of red blood cell interior, C_{rbc} is the capacitance of red blood cell membrane and L is the relative volume of blood cells in the micro veins of the lobule.

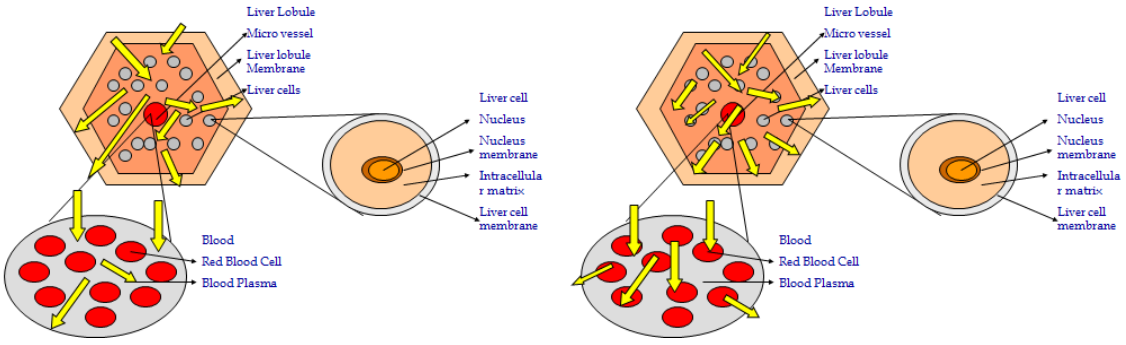

Figure 3.6. Liver lobule model. (left) low frequency behavior of liver lobule (right) high frequency behavior of liver lobule.

The lobule complex resistivity value is represented by:

$$Z_{lobule} = Z_{mv} + N\frac{R_{lecm}+i\omega R_{lecm}C_{lc}Z_{lc}}{1+i\omega C_{lc}(R_{lecm}+Z_{lc})}, \tag{3.6}$$

where R_{lecm} is the resistance of lobule extracellular matrix, Z_{lc} is the complex resistivity of liver cell, C_{lc} is the capacitance of liver cell membrane, N is the number of liver cells in the lobule and Z_{mv} is the complex resistivity of micro veins in lobule.

At the tissue level, the existence of vessels can be modeled when required (Figure 3.7). The vessel has a similar structure to the central vein represented by:

$$Z_{vessel} = KZ_{blood} = K\frac{R_{plasma}+i\omega R_{plasma}R_{rbc}C_{rbc}}{1+i\omega C_{rbc}(R_{plasma}+R_{rbc})}, \tag{3.7}$$

where R_{plasma} is the resistance of blood plasma, R_{rbc} is the resistance of red blood cell interior, C_{rbc} is the capacitance of red blood cell membrane and K is the relative volume of blood cells in the vessel of the tissue. The tissue level is the final output level of the model which incorporates the vessel (if any) with the liver lobules. The equation to represent the complex resistivity of the tissue is:

$$Z_{tissue} = Z_{vessel} + M\frac{R_{tecm}+i\omega R_{tecm}C_{lobule}Z_{lobule}}{1+i\omega C_{lobule}(R_{tecm}+Z_{lobule})}, \tag{3.8}$$

where R_{tecm} is the resistance of tissue extracellular matrix, Z_{lobule} is the complex resistivity of liver lobule, C_{lobule} is the capacitance of liver lobule membrane, M is the relative volume of lobules in the tissue and Z_{vessel} is the complex resistivity of vessel in tissue sample.

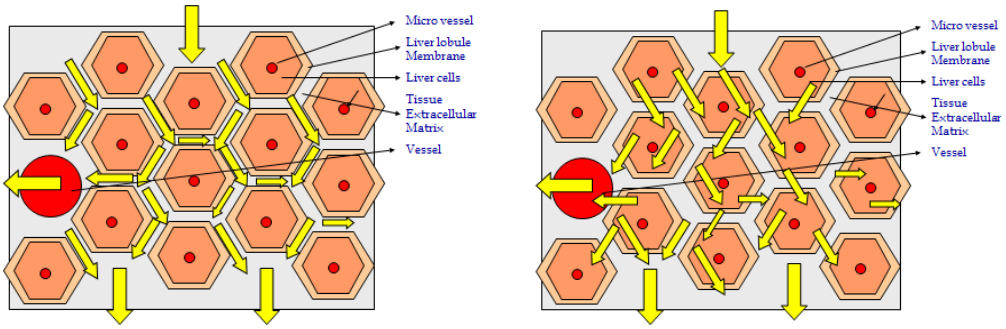

Figure 3.7. Liver tissue model. (left) low frequency behavior of liver tissue (right) high frequency behavior of liver tissue.

3.4 Simulations and results

Computer simulation was performed using Matlab. The permittivity of the model with respect to frequency was computed and the output was fitted to experiment results from Gabriel (1996). Gabriel fitted the data in a summation of four classical model of Cole-Cole equation. The magnitude vs. frequency plot (Bode plot) from both models is shown in Figure 3.8. Results were presented in log scale for a more compact visualization. The solid line represents the fitted results from Gabriel et al., while the dashed line the output of our proposed model. It can be observed that our model is able to fit the data better.

The parametric values to the model are available in caption of Figure 3.8 and are obtained using a model fitting algorithm in Matlab. It is evident that the model is able to exhibit similar trends to that of the experiment results. The structure of the proposed model provides a physical explanation and analogy to the actual tissue structure, often lacking in various models depicting bioimpedance dispersion.

A change in the permittivity values of the β and γ dispersion allows the inference of changes in tissue structure during RF ablation. The γ dispersion is due to polarization of water and extracellular matrix content in the soft tissue. Hence, it is important for the model to exhibit changes due to corresponding structural changes. The change in blood volume is the most important structural change for the purpose of this model.

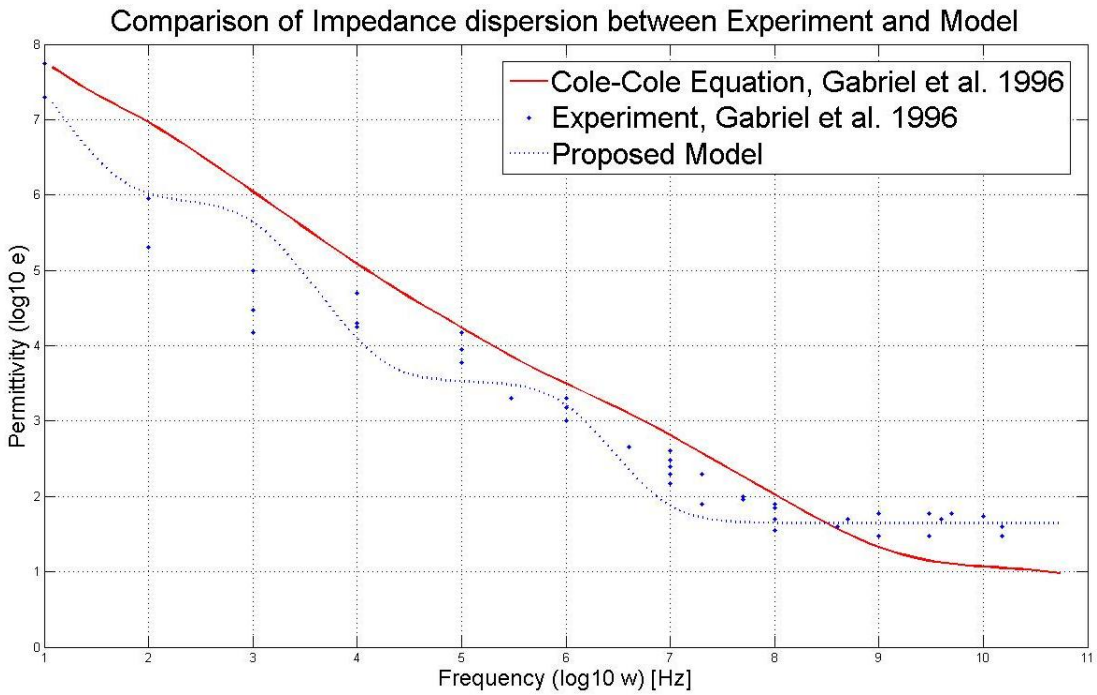

Figure 3.8. Plot of the permittivity magnitude vs frequency. Dashed line representing proposed model output, solid line representing Cole-Cole model output. R_{icm}=450Ω, C_n=0.0000000001F, R_n=600Ω, L=0.4, N=0.3, K=0.1, M=0.4, C_{lc}=03nF, R_{lecm}=35000Ω, Rl_{plasma}=2000Ω, R_{rbc}=1500Ω, C_{rbc}=0.035nF, C_{lobule}=800nF, R_{tecm}=12500Ω

Figure 3.9 shows the model output with decreasing blood volume. The arrow indicates the decreasing of blood flow in the model. The gamma dispersion was almost diminished and the Bode magnitude plot exhibits mainly the β dispersion. This result is encouraging as it is able to successfully mimic the effect of a reduced blood volume. A reason for the diminishing of the γ dispersion is that blood contains a large amount of

water in the plasma material and hence a reduction in blood volume affects the γ dispersion magnitude. Since the extracellular matrix contains water, the gamma dispersion does not level out completely. From simulation, we observed that the total permittivity of the system increased due to the reduced blood flow. This is due to the conductive nature of water, and hence a reduction of it results in increased permittivity.

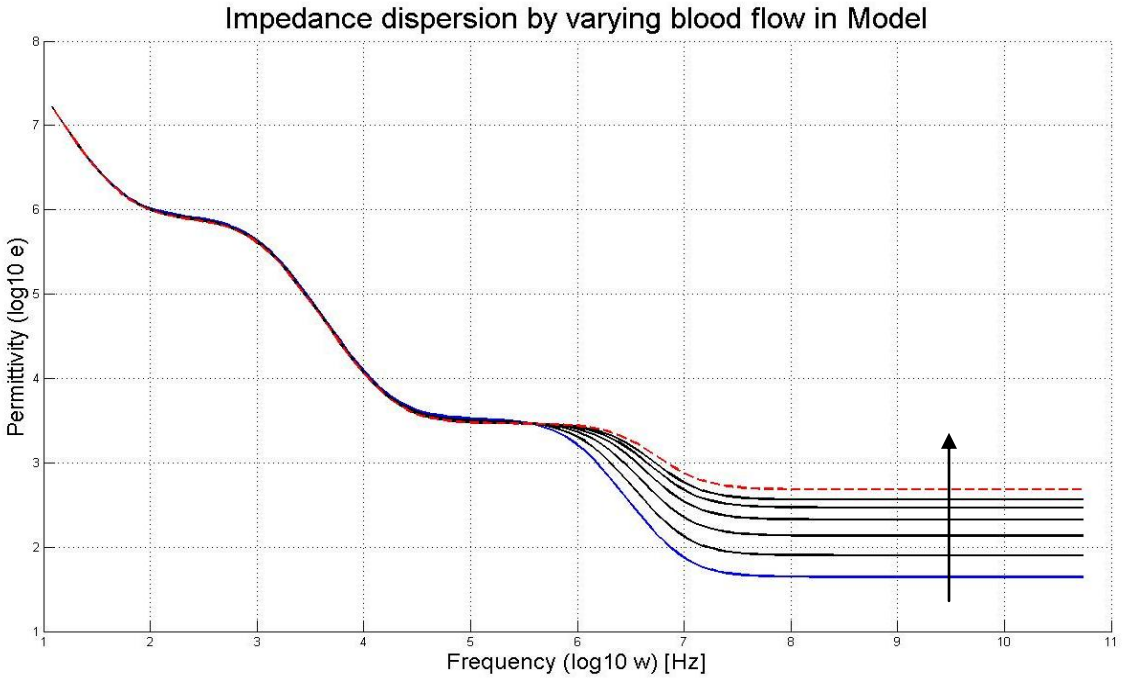

Figure 3.9. Plot of permittivity response with decreasing blood flow. Red line represents no blood flow in model.

3.5 Discussion

It was observed that the proposed model fits the experimental results obtained by Gabriel well, with slight discrepancies near the alpha dispersion region. The model outperforms the Cole-Cole equation proposed by Gabriel (1996), which made used of an Excel spreadsheet to fine tune the curve fitting parameters. Linear least square methods were not implemented as they observed that conventional linear least square techniques

are biased towards low frequency outputs. The model fitting used for the proposed model was an iterative code to minimize the maximum discrepancy between our model and Gabriel's data.

The α parameter, which accounts for depressed circular arc in the complex plane, in Cole-Cole model is not required in the proposed model. There is no theoretical explanation behind the parameter and hence the author did not find it suitable to be incorporated into the model. Nonetheless, the output of the proposed model is close to the experiment data by Gabriel. We are satisfied with the performance of the model with comparison between two sets of data by different groups.

The proposed model made use of the same number of parameters to the one used by Gabriel, a total of 14. However, 2 parameters (K and L) of the proposed model can be changed to account for different tissue perfusion samples. In addition, parameters M and N can be tweaked to account for tissue structure variability. This model could account for the variability in tissue properties so commonly encountered in actual measurements.

In clinical setting, bioimpedance measurement of liver tissue can be obtained during surgery using a bioimpedance spectroscope. The results are fitted with this model with bounded values for parameters such as cell resistance and capacitance. The parameters can provide an insight to the amount of blood and water present in the target region as well as cell distribution. This could be used as a blood sensing technology in reducing blood loss during various surgeries such as liver resection (hepatectomy). While further work remains to be done, the model has the potential to possibly explain for variations in different tissue sample due to its inherent geometrical nature.

The proposed bioimpedance model is able to model liver bioimpedance more accurately than the classic models. In addition there is potential in the usage of the model in the development of a new technique for blood flow imaging. This technique enables blood flow to be detected by electrodes with large sensing area. Computer simulation of the multi-scale model demonstrated the capability of this new approach for blood flow imaging. We have conducted in-vivo experiments and are conducting ex-vivo experiments to further validate the model. With a bioimpedance analyzer, the impedance of tissue sample can be measured over the frequency spectrum. Details pertaining to blood flow can be extracted from experimental data in accordance with the proposed model.

Although the computational model was developed for liver tissue bioimpedance dispersion, the multi-scale model is applicable for heterogeneous tissue characterization in general. The performance of the model was compared to the experimental data by Gabriel with satisfactory fit and provides a physical explanation for the dispersion characteristics.

Chapter 4

RF ABLATION AND MECHANICAL PROPERTIES

Huang WH, Chui CK, Kobayashi E, Teoh SH, Chang SKY, 2011. Multi-scale model for investigating the electrical properties and mechanical properties of liver tissue undergoing ablation. Int J Comput Assist Radiol Surg, 6(5), 601-607.

This chapter contains work from the above cited journal paper which was published in 2011. This chapter describes work in building a model to mimic the RF ablation process. This chapter reports a multi-level tissue model that we have developed to investigate the changes in electrical and mechanical property of ex-vivo liver tissue during RF ablation. The output from the model is correlated to changes in mechanical properties in a 3D correlation plot. Section 1 introduces RF ablation and the different methods used for quantification. Section 2 introduces the proposed model and section 3 describes the experiments. Section 4 discusses the work and highlights future work in the field following by a concluding paragraph.

4.1 RF ablation

RF ablation causes tissue injury and denaturalization which results in changes in tissue modulus (Jiang 2007). Mechanical properties of tissue can be used as a measure of cell injury due to RF ablation in addition to other properties such as electrical impedance

and optical properties. It is inevitable that the denaturalization of tissue caused by temperature results in tissue structure changes and hence changes in physical properties. Magnetic Resonance Elastography (MRE) is a choice for quantifying mechanical properties in-vivo. MRE is a noninvasive medical imaging technique which combines MRI images with propagating sound waves into a map (elastogram). The elastogram shows the stiffness distribution of body tissue for the area of concern. The technique can be used to measure stiffness of tissue to differentiate between normal and ablated tissues.

Greenleaf et al (2007) developed a noninvasive technique to measure liver tissue stiffness by inducing ultrasonic radiation force to induce shear waves for propagation. The propagation speeds of the waves were measured as a function of frequency. The measured dispersion curve was then fitted to the Voigt model in determining tissue elastic and viscous moduli.

Many studies (Moffitt 2002, Walsh 1989) concluded differences in mechanical properties between healthy tissue and tissue subjected to hyperthermia treatment. It was concluded that the ultimate strength of native liver is higher than that of the thermally damaged liver. Kiss et al (2004) investigated the viscoelastic properties of normal and thermally damaged canine liver tissue and the results fitted to the classic Kevin-Voigt model and Kelvin-Voigt Fractional Derivative model. Kelvin-Vogit fractional Derivative model was concluded to exhibit better fit to experiment data. Obvious differences were observed between normal and thermally damaged tissue exhibiting viscoelastic properties. The various studies in mechanical properties draw an interesting insight into the causal relationship between RF ablation and mechanical properties (tissue structure), and also its vice versa.

Dumas (2008) used the myocardial electrical impedance as a predictor of RF lesions and reported that the tissue impedances increases with complete ablation This also justifies our hypothesis of a changing electrical property of the liver while undergoing the Radio-frequency ablation process. Solazzo (2005) reported a strong relationship between background tissue conductivity and RF heating hence further justifying the relationship between tissue electrical property and the heating process. Santago (2009) studied the effects of freezing on mechanical properties of bovine liver. A single bovine liver was divided into two halves, previously frozen and normal, and uniaxial tensile test was done. It was observed that average failure strain was different between the two.

Many before us proposed electrical models for the liver tissue. However, such tissue electrical models are only applicable for electrical property detection (as per section 3) due to frequency differing voltages and do not model changes in cell structure due to any dynamic physical process. A related work is done by Vasilkoski (2006) whom proposed an equivalent circuit for a single cell electroporation process with the integration of a variable resistor to represent opening of pores.

4.2 Proposed model

4.2.1 Model description

The proposed RF ablation model of the liver tissue consists of extracellular structure and individual cells (Figure 4.1). The individual liver cells are modeled as a capacitor in parallel with that of a resistor. The cells are modeled in parallel with each other as they are subjected to the same RF signal at the same time. The extracellular structure model connecting all the cells in a tissue is similar to that of individual cell. It is

important to note that the number of cells in the model corresponds to the size of the tissue sample and can be varied for difference sample sizes. Hence, it presents a realistic model of how size of the liver tissue sample affects the model responses of the liver tissue sample. The extracellular structure however remains a constant size as it is usually of smaller impedance value (conducting) and thus has a smaller impact on the overall response of the model.

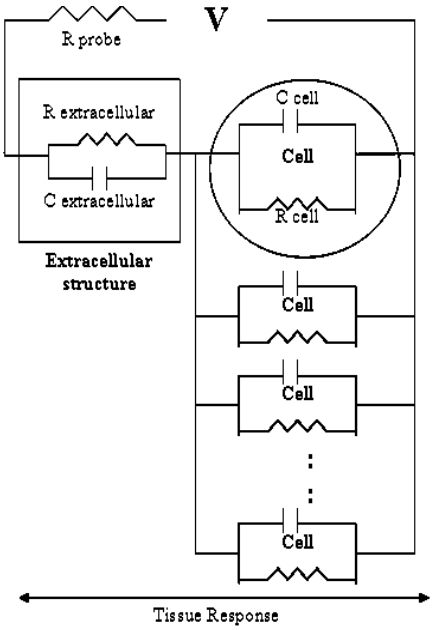

Figure 4.1. Proposed electrical equivalent model

The impedance response to the model is the tissue voltage which is the potential difference across the liver tissue when a RF signal is passed through the tissue. The tissue voltage is defined as the quotient of voltage of tissue by the voltage of the whole circuit as shown in Figure 4.1. The tissue voltage response can be correlated to the mechanical property of liver tissues which will be further elaborated in later sections. Laplace transform is used to evaluate the tissue voltage across all the cells. The mathematical equation of the model in the Laplace Domain is available in Equation 4.1. R_e represents

the resistor value of the extracellular matrix while R_c represents the resistor value of the cell. C_e represents the capacitance value of the matrix while C_c represents the cell capacitance. The constant n is the number of cells in the tissue sample and hence can be user specified.

$$\frac{V_{Tissue}}{V_{applied}} = \frac{\frac{R_e}{1+s\tau_e} + \frac{R_e}{n(1+s\tau_c)}}{R_p + \frac{R_e}{1+s\tau_e} + \frac{R_e}{n(1+s\tau_c)}}$$

$$\text{for } \tau_e = R_e C_e \text{ and } \tau_c = R_c C_c \qquad (4.1).$$

4.2.2 Simulation

Computer simulation was performed on the model implemented using MATLAB to simulate the response of the model in the time domain. The results of simulation are available in Figure 4.2. The simulation results are normalized to a constant value with the response at *t*=0 being the initial impedance of the liver tissue. The initial impedance is not representative of the actual impedance of the sample, but as a value to fit the response to experimental values. Initial impedance value is around 0.1ohm and varies slightly between sample sizes.

A key component of the simulation is the settling time of the model for different sample size. The settling time in the simulation is the amount of time required for the impedance response to stabilized within 2% of steady state value and hence is analogous to the tissue being fully ablated. It is evident that with a larger sample size, the amount of time required for the ablation process increases and is observed from experimental data.

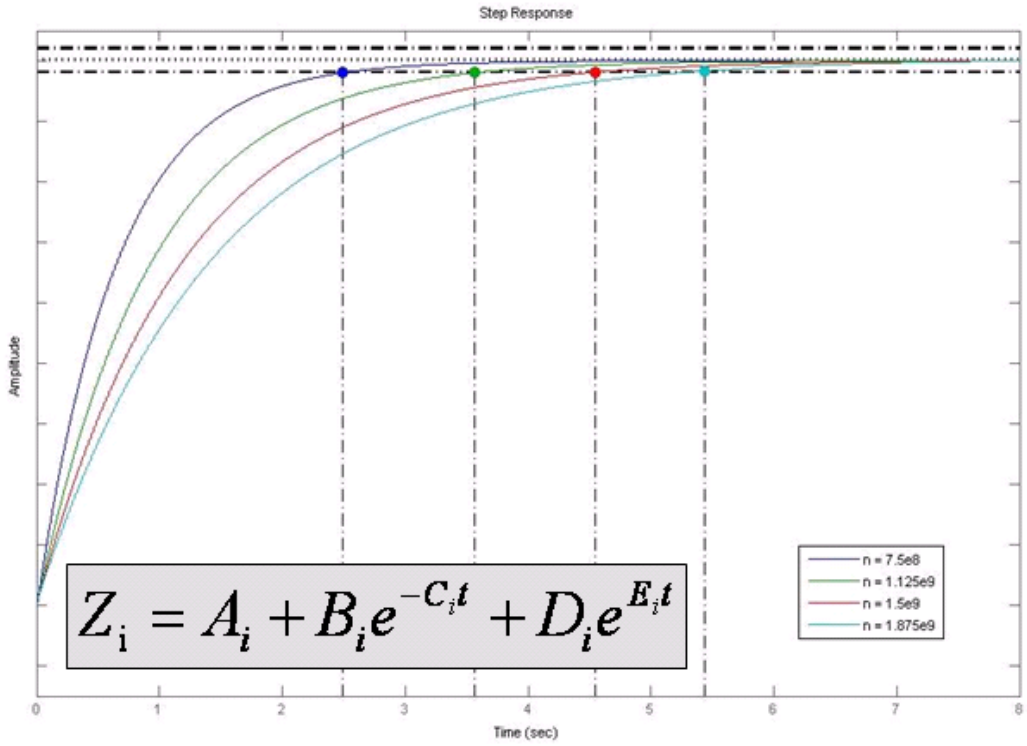

Figure 4.2. Simulation of proposed model

4.2.3 Implementation

Prognostication of liver tissue properties can be useful in the development of RF ablation surgical and simulation devices. Knowing the electrical property of the tissue aids the determination of RF pulse duration (for minimum cell necrosis before coagulation) to minimize the affected ablated area, thus reducing the invasiveness of the procedure. On the other hand, prediction of the changes of mechanical property of liver tissue helps in the development of the RF ablation device in the design of cutting mechanism and its related parameters.

The following section discusses how the proposed model can be used to correlate the electrical property with that of mechanical property, and hence prediction of changes in electrical and mechanical property during the ablation process. The work flow of the

model implementation is available in Figure 4.3. During the process of Radio-frequency ablation, cell necrosis and moisture losses occur due to Joule heating induced by the RF waves. The changes in micro and macro structure of the liver tissue results in a change in electrical property as predicted by our model. By correlating our model results with experimental results from mechanical load tests, a correlation can be made between the electrical and mechanical properties of the liver tissue, with the changes in properties due to the ablation process. The correlation between the two properties enables an estimation of the relationship between the two and thus allowing optimization of the prototype parameters. Optimization of the prototype parameters ensures that the device is used with minimum invasiveness to the patient.

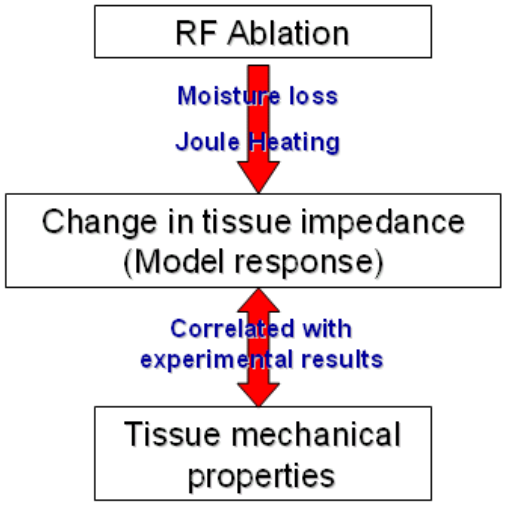

Figure 4.3. Workflow of implementing model

4.3 Experiments

4.3.1 Experimental setup

The Rita 1500X RF Generator (Figure 4.4) which is a 100W rated generator is set to impedance-controlled mode during usage. Impedance controlled mode controls and stops the ablation process by sensing tissue impedance in between the RF needles. This provides us a benchmark to classify tissue samples as fully ablated by maintaining constant impedance for liver tissue between the RF needles. The halt of RF wave generation also act as an experimental data for the time required to ablate a certain volume of liver tissue sample.

Figure 4.4. Rita 1500X RF generator

The setup of mechanical testing consists of a test rig (Figure 4.5), developed by the group for 3-axis movement. The actuation of the test mount is controlled precisely by Labview software and has a compression motion actuated by precision screw at 1mm/s. A 15N UF1 Isometric force sensor that was mounted onto the test rig was connected to the PC for feedback control and data collection. Histoacryl® by B Braun Aesculap Surgical glue was used to attach tissue specimen to tissue holder.

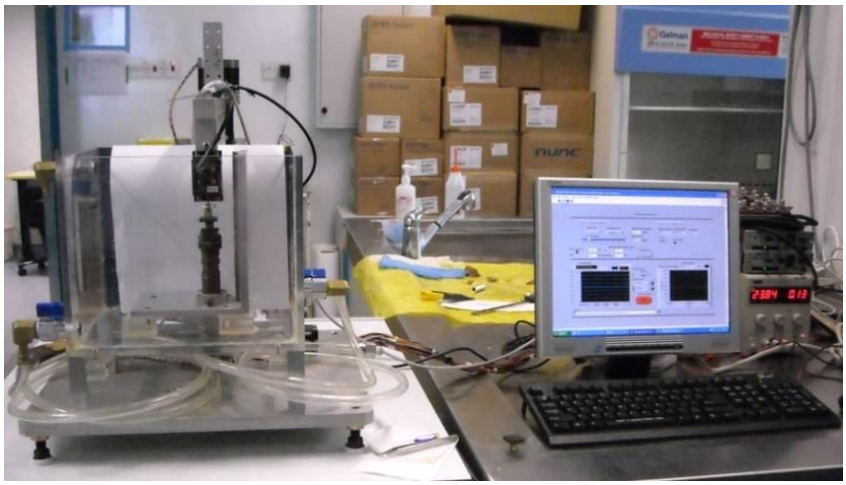

Figure 4.5. Test rig and controlling PC with Labview

Two experiments were conducted to study, namely; relationship between tissue sample size and the time taken for ablation; and the relationship between ablation time and tissue mechanical property.

4.3.2 Tissue sample size vs. time for ablation

In this experiment, the relationship between tissue sample size and ablation time was investigated. The motive of the experiment is to verify the accuracy of the electrical equivalent model proposed in earlier section.

Fresh porcine liver was used for the experiment. The specimens were dissected into different volume and the prototype was used to induce ablation to it. The time taken for the ablation process was recorded and the mean time was computed. The experimental results were compared to that of the settling time in the simulated results and the comparison chart is available in Figure 4.6.

Volume of specimen (m^3)	3.142E-06	4.712E-06	6.283E-06	7.854E-06
No. of Cells in specimen	7.500E+08	1.125E+09	1.500E+09	1.875E+09
Average Time (s)	2.550	3.465	4.513	5.437
Simulation results (s)	2.49	3.56	4.54	5.44
Difference (s)	0.060 **(2.35%)**	-0.095 **(-2.74%)**	-0.027 **(-0.60%)**	-0.003 **(-0.06%)**

Figure 4.6: Comparison between experimental data and simulated results

Comparison shows similarity in settling time of the simulation and the ablation time in the experiment for a known tissue sample. It can be seen that the maximum differences between the two results was 2.74% which is close enough for us to conclude that the accuracy of the model is sufficient. Although more work is required to fully verify the validity of the model, this initial result showed that it is viable to continue with the next step of model implementation. Additional experiments can be repeated for further validation of the model. Experiments can be conducted in a controlled ambient temperature in ensuring a constant heat loss from the sample. The next step is to investigate the relationship between the ablation time and the mechanical property of the liver tissue sample, and then establish a relationship between the ablation time, the electrical property and the mechanical property of the tissue sample.

4.3.3 Ablation time vs. tissue mechanical property

Experiment was conducted to determine how the mechanical property of the tissue samples change with ablation time. Data collected permits understanding of how

mechanical property changes and also reveals probable correlations between mechanical and electrical properties.

Specimens of standard size and shape were obtained from freshly excised liver (3.142E-06m^3). The specimens were subjected to RF ablation for different duration i.e. 0.5s, 1.5s, and 2.5s. The ablation time affects the degree of cell necrosis and heating the samples were subjected to. The ablated or partially ablated samples were put into the test rig and compression test was done at a strain rate of 1mm/s. The compression test was done up to 50% strain and data was collected.

The data points were plotted and fitted with the Combined Energy Function by Chui (2004). The Combined Energy Function is a strain energy function that has been used to model the nonlinear stress-strain relationship of liver tissue. . It consists of fewer constants for fitting compared to the often cited Mooney-Rivlin function. The ease of fitting due to a smaller number of constants makes it the choice for our fitting of the stress-strain relationship for ablated tissue. The Combined Energy Function equation is available as

$$\sigma = \left(2 + 2\varepsilon - \frac{2}{(1+\varepsilon)^2}\right)\left(\frac{C_1 C_2}{\left\{6C_2 + 2 - 2C_2(1+\varepsilon)^2 - \frac{2C_2}{1+\varepsilon}\right\}}\right) + C_3 \qquad (4.2).$$

The Stress-Strain relationship was plotted as shown in Figure 4.7.

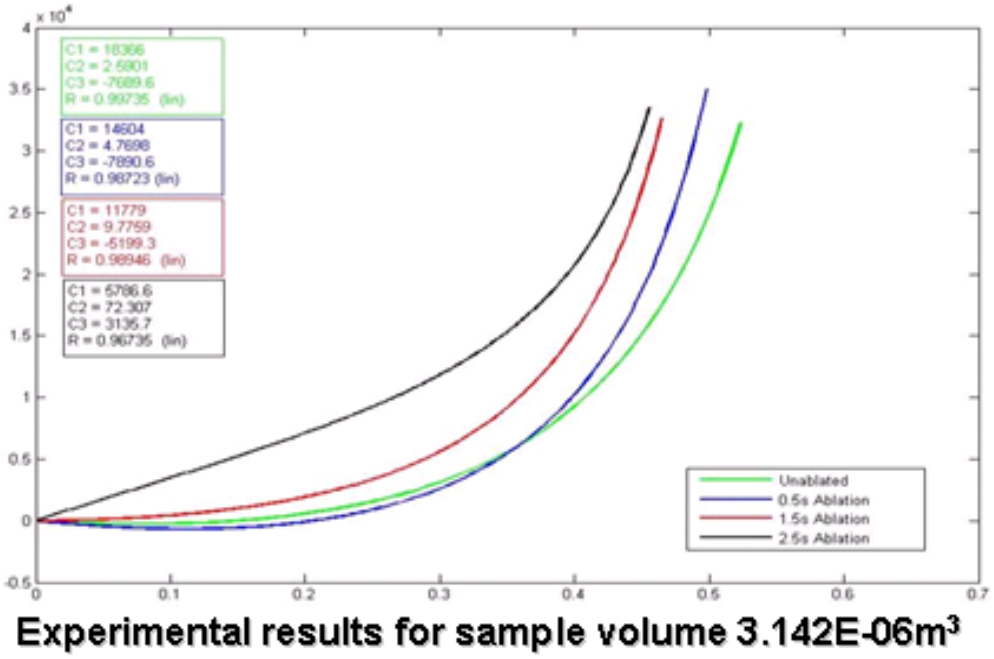

Figure 4.7. Compression test results fitted with combined energy function

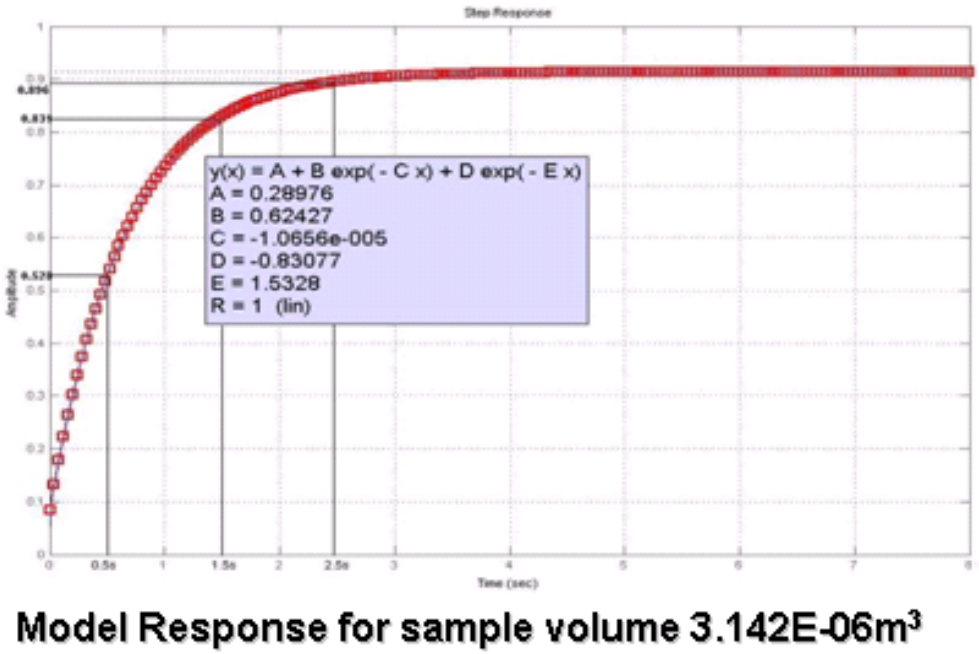

Figure 4.8. Electrical property response with ablation time

With data between the mechanical properties and ablation time collected, correlation was done to the model simulated electrical property (Figure 4.8) and the experimentally obtained mechanical property into a 3D surface (Figure 4.9). This 3D surface plot can be used for visualization of how electrical and mechanical properties changes. With the 3D surface, it helps in the prognostication of tissue properties during the ablation process.

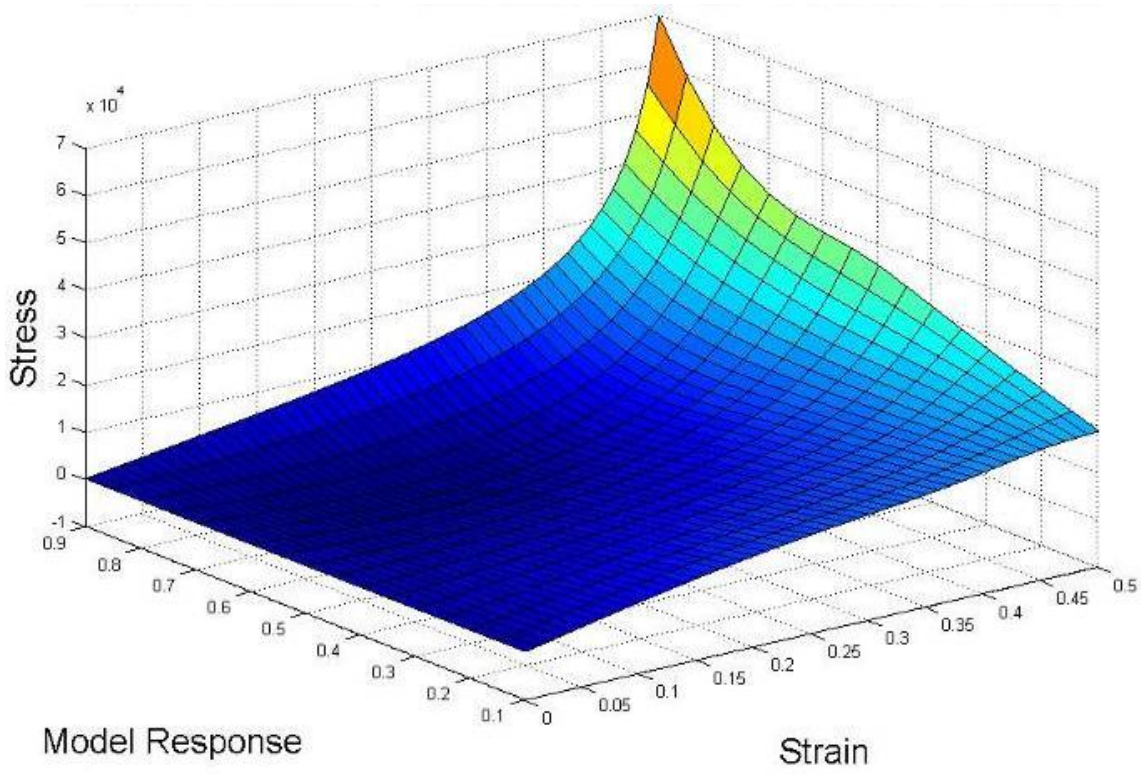

Figure 4 9. 3D plot of mechanical and electrical properties

4.4 Discussions

The 3D plot provides a basis to understanding how the two properties change with respect to each other during the ablation process. Both properties are important in optimizing the parameters of the ablation-resection prototype. The mechanical properties determines how fast the knife blade should be actuated for minimal invasiveness while the electrical property determines how long should ablation be done prior to resection.

The model also enables user to specify the size of the sample subjected to ablation. This is useful for users when they only require ablation to a small affected area. Hence it reduces the possibility of an oversized affected zone. The model enables user to predict duration of ablation for a given tissue size hence is useful for operational planning. However, more experiments have to be performed for different liver tissue sample sizes for the 3D plot.

Prognostication of changes in mechanical properties of tissue aids in optimizing parameters for RF surgical and simulation devices. It also helps in our understanding on how mechanical properties changes when the tissue is subjected to ablation. The change in mechanical properties in the event of RF ablation is important for tissue modeling. The electrical model can also be used to reinforce the modeling of joule heating which is often used in hyperthermia modeling that assumes constant tissue impedance. The model of varying tissue impedance will be useful for a more accurate hyperthermia model for medical treatments and predictions.

Relevant tissue impedance imaging methods may be relevant to the proposed electrical equivalent model. The model can be used as a basis for impedance imaging methods such as the Electrical Capacitance Tomography (ECT) for simulation. The

tissue model can be taken as the dielectric material with changes in dielectric constants affecting the permittivity values. An image can be constructed by applying an inverse to the dielectric equation. ECT can be used effectively to predict the state of coagulation of the liver tissue which serves as a live feedback monitor for surgeons. It can also be used for detection of possible blood vessels which are not coagulated by the ablation process due to its capability of a two phase imaging.

A short coming of the proposed model is that stochastic errors may cause discrepancies between liver and tissue sample location. Hence, more experiments will be needed to overcome the possible random errors. Although further investigation is required to validate the electrical model that correlates the electrical and mechanical properties, this study showed that the proposed model is viable and can be a first step towards a unified model for investigating liver tissue ablation and division.

Further work can be done to understand the underlying relationship of how changes in micro-scale affect properties in the macro scale. This aids in our understanding of how electrical and mechanical properties are correlated and thus enables us to better predict them. It is also desirable to build a more realistic model in predicting impedance changes due to ablation by incorporating variations such as tissue perfusion, temperature transfer and thermal conductivity. The properties form a close loop relationship with RF ablation as they are both causal and affected in the process.

In this chapter, we describe multi-scale model to simulate the electrical property of the liver tissue undergoing RF ablation. Simulation work was done for the model and mathematical model was established in both the Laplace and time domain. Experimental work was done to verify the proposed model with closely matched results concluded. The

proposed model was concluded to be suitable for modeling the changes in electrical property of the ablation process.

Another experiment was done to correlate ablation time to mechanical properties of the liver tissue which underwent different ablation time. The experimental data of the mechanical properties were correlated with that of the predicted electrical property of the simulated model. This presents a 3D relationship established between the Stress, Strain and Impedance of the ablated liver tissue.

The proposed model presents a new approach in predicting mechanical properties of liver tissue by the correlation of it with electrical properties. This enables us to predict possible mechanical properties from electrical properties and vice versa. The established model and correlations enables optimization of RF assisted liver resection surgery and the operational parameters for the development of RF ablation devices.

Chapter 5

LARGE TUMORS KINETICS

Huang WH, Chui CK, 2012. A Radio-Frequency Ablation Planning System using Stochastic Finite Element Method. IEEE/SICE International Synopsium on System Integration.

This chapter introduces a new proposed method in large tumor RF ablation surgical planning. Stochastic finite element analysis was integrated with surgical planning for more realistic results. Section 1 introduces large tumor treatment and the second section describes existing planning system. Section 3 introduces Stochastic Finite Element (SFE) method and section 4 demonstrates the use of the method in a RFA planning system. Lastly, the concluding section presents results and discussions.

5.1 Large tumor treatment

Surgical resection is the gold standard for treatment of hepatic tumors. Ten percent of colorectal liver metastases patients are potential candidate for hepatic resection, otherwise known as hepatectomy. Hepatectomy is a viable treatment for 20-30% of hepatocellular carcinoma patients with non-cirrhotic liver and lower in cirrhotic liver (Tranberg 2004). Radio-Frequency (RF) ablation serves as a good alternative treatment for liver tumors and are preferred over other hyperthermia treatments due to its low invasiveness, simplicity and cost effectiveness (Ni 2005). It can be performed in a minimally invasive way, percutaneously or laparoscopically. RF ablation is the

application of a high frequency (550KHz) electric voltage within a target biological tissue which generates high current density and hence ionic agitation and frictional heating. The increase in temperature leads to coagulative necrosis in tissue (Haemmerich 2003). Catheters used for RF ablation are often needle electrodes for high current density and can be found in two forms; monopolar or bipolar electrodes. Monopolar electrodes work on the principle of a single polarity electrode with a large grounding pad attached to patients while bipolar electrodes are electrode pairs with dual polarity hence do not require a grounding pad. The electric field lines that are induced from the electrode tip by the applied voltage causes an electric force on the charged ions within the electrolytic medium of the liver tissue. This induced force produces a motion that causes ions in the tissue to rub against the surrounding fluid medium, causing friction and thus frictional heating.

There are limitations to the size of hyperthermia treatment zone for RF ablation. Joule heating, which is the primary heating mechanism, decreases rapidly with increasing distance from the electrode-tissue interface. Ablated tissue adds further resistance to current flow and hence reduces the efficiency of the method. Secondary heating mechanism is due to bioheat transfer. Several works related to catheter design were done to maximize the hyperthermia zone of RF ablation for large tumor ablation (Ni 2005). Many methods were developed such as saline injection (Livraghi 1997) for increased electrical conductivity, cooled electrodes to reduce charring (Goldberg 1996), bipolar array to increase treatment zone (McGahan 1996), etc. However, recurrence rate is high especially in the case of large tumors. Chen (2004) explained the higher recurrence rate to be the inability to determine the optimal number of ablations and the exact location of

electrode position. These large tumors require overlapping electrode placement to achieve complete destruction and adequate ablation margin to reduce recurrence.

This chapter discusses the potential of integrating stochastic finite element simulation in surgical planning for accurate large tumor ablation. With the usage of stochastic finite element methods, the temperature of target tissue zone can be simulated. Stochastic finite element method is performed by input of vasculature information and other physical properties randomly chosen from a normal distribution. The reason for a randomized parameter selection is to account for non-homogeneity in actual tissue samples. Vasculature information can be obtained from pre-surgical imaging such as Computed Tomography or Magnetic Resonance Imaging (MRI).

5.2 Large tumor planning

Large tumor surgical planning is crucial in ensuring low recurrence rate in RF ablation treatments. Past studies indicated the importance of overlapped ablation zones and sufficient tumor-free margin in prevention of recurrence and failure (Chen 2004, Dodd 2001, Livraghi 2000). Dodd (2001) proposed one-ablation, six-ablation and 14-ablation model for large tumor surgical planning. The ablation spheres were overlapped in an optimized manner for maximum volume with a 1cm tumor free-margin. Chen (2004) proposed methods for RF ablation planning by making use of mathematical protocol to optimize the process. Regular tetrahedron overlapping modes and regular prism overlapping modes were proposed for tumors of different sizes. The aim of the method was to achieve safety margin of 0.5cm with overlapping heated zone in ensuring

sufficient tissue temperature for tumoric cell necrosis. For both works, the ablations were assumed to be a perfect sphere and consistent in shape.

Khajanchee (2004) studied the relationship between tumor size and smallest number of ablation for complete tumor destruction. The team concluded that the minimum number of ablations increases dramatically with tumor size. This is due to the optimization method, which is geometrical in nature, being vastly affected by any small change in position of ablation spheres. A small increase in tumor size will result in small volumes of un-ablated tumor, thus requiring more ablation spheres to be used.

While the above mentioned methods provide a guide to the clinicians, the assumption of a constant ablation sphere is unrealistic. Studies showed the variability of RF ablation lesion for a single device, with variation in size and shape in a large percentage of samples (Montgomery 2004, Stippel 2004). Hence, lesion variation should be considered as part of ablation planning strategies. Lesion variations were not considered in the ablation planning for the cited work above and are not present in literature to the author's best knowledge.

Various literatures demonstrated Finite Element simulation for RF ablation in liver tumors. Haemmerich (2001) investigated the differences between monopolar and bipolar RFA with the use of a finite element model. The Electric field distribution of the target tissue zone is govern by

$$\Delta \cdot E = \frac{\rho_c}{\varepsilon_0}, \tag{5.1}$$

where ρ_c is the charge density, E is the electric field and $\varepsilon_0$the permittivity.

A modified Pennes bioheat equation was used for RF ablation simulation as

$$\rho c \frac{\partial T}{\partial t} = \nabla \cdot k\nabla T + J \cdot E - \rho_{bl} c_{bl} \omega_{bl} (T - T_{bl}), \tag{5.2}$$

where ρ is the density, c is the specific heat capacity of material, T is the temperature, k is the thermal conductivity, J is the current density, E is the electric field, ρ_{bl} is the blood density, $c_{bl}$is the blood specific heat, $\omega_{bl}$is the blood perfusion rate and T_{bl} is the blood temperature.

It was concluded that the bipolar method creates larger lesions and is less dependent on local inhomogeneity in liver tissue. Chang and Nguyen (2004) attempted to model RFA process in soft tissue by means of a two dimensional finite element model. The model takes into account both the temperature and electrical conductivity dependence of the RFA process with respect to the tissue. The model has a close loop, self-updating structure consisting of the Specific Adsorption Rate (SAR) - the amount of energy absorbed by the tissue from the ablation needle, the Penne's bioheat equation, for updating of tissue temperature, updating thermal conductivity of tissue and Arrhenius equation to update the tissue damage and perfusion related. Ahmed (2008) used an established computer simulation model of RFA to characterize the combined effects of varying perfusion, and electrical and thermal conductivity on RF heating. The varying electrical and thermal conductivities are used to represent tissue, fats and saline injection. The different parameters were changed to model the effect of RF heating in different scenarios.

Solazzo (2005) studied the effect of a varying background electrical conductivity to RF heating effectiveness and concluded that there is a strong relationship between background tissue and RF heating. Arkin (1994) reviewed the different models proposed in modeling heat transfer in blood perfused tissue. The model aids in better prediction of hyperthermia procedure which is relevant to the RFA technique we are studying. Due to

the complex morphology of living tissues, hyperthermia modeling is often difficult and requires simplifying assumptions to be drawn. It was concluded that Pennes' model might still be the best practical approach.

Stochastic Finite Element (SFE) method is the combination of statistical methods with deterministic physical models to account for variation and noise in simulation. The method relies on a statistical probability density distribution for parameter values which mimics the inherent biological tissue structural variations. Stefanou (2009) discusses the various frameworks of SFE method in the field of analysis of uncertain systems in which uncertainty often occurs to the inputs of the system. Although most inputs are non-Gaussian in nature, many works has inputs often described to be statistically Gaussian. The Gaussian assumption is simple and convenient due to the lack of experimental data. In addition, the Gaussian random fields are naturally occurring due to Central limit theorem.

While the method was mainly used in structural engineering (Beck 2006, Argyris 2002, Baroth 2006, Kiureghian 1998), the method is slowly finding its way into biomedical applications. Fuentes (2012) used SFE method in a stochastic form of Penne's Bioheat equation integrated with a Kalman filter to provide temperature field estimates in time of data loss. Clinical data was collected with the use of Magnetic Resonance Temperature Imaging (MRTI) with partial temperature information removed. The residue data act as a reference to the Kalman filter and results simulated shows accuracy with no effect of Kalman filter on known data points.

Hu (2010) studied the behavior of the human placenta tissue on impact, which is the highest cause of fetal death in accidents, with stochastic finite element analysis of a

visco-hyperelastic model. Material of statistical nature was used with results showing good agreement with actual data and simulated results. Gao (1998) employed stochastic finite element analysis to simulate noise and scattering present in time-resolved optical tomography imaging. Photon propagation scattering and noise from measuring device both contributed to variations in data and hence uncertainty. The method allows a forward problem simulation for verification of their proposed inverse problem solving utilizing Tikhonov-Miller regularization method.

Delalleau (2011) investigated the usage of stochastic method in solving inverse optimizing problem. Elastic properties of skin were modeled by two model: a classic single layer hyperelastic model and a double layer neo-Hookean potential model. The purpose of the study was to observe the performance of such stochastic optimization method and concluded that there is potential in the novel approach.

5.3 Stochastic finite element methods

Various RF ablation simulation methods were reviewed in the earlier section. However, a common short-coming is the assumed constant physical properties for all tissue samples. The assumption of constant physical properties in liver sample is inaccurate due to variation in micro structure and micro perfusion. In addition, liver tumors are angiogenic in nature thus altering perfusion state around the tumor. Variations in physical properties such as electrical conductivity, thermal conductivity, perfusion rate and density affect the final output of the simulation (Solazzo 2005, Arkin 1994) and should not be assumed to be identical.

We propose a Stochastic Finite Element (SFE) method for Bi-Polar RFA simulation. The method relies on a statistical probability density distribution for parameter values which mimics the inherent tissue structural variations. The probability of parameter within an interval [a,b] is given by

$$P(a \leq X \leq b) = \int_a^b f_x(x)dx\,, \tag{5.3}$$

where $f_x(x)$ is the probability density function of variable x. The governing electric field distribution of the target tissue zone in (5.1) is hence given by

$$\Delta \cdot E = \frac{\rho_c}{\varepsilon_{0,r}}\,, \tag{5.4}$$

where subscript r represents a random parametric value following a normal distribution. The tissue permittivity is randomly chosen from a normal probability density function. The Penne's bioheat equation in (5.2) is modified as follows:

$$\rho c \frac{\partial T}{\partial t} = \nabla \cdot k_r \nabla T + J_r \cdot E - \rho_{bl} c_{bl} \omega_{bl,r}(T - T_{bl}). \tag{5.5}$$

The method is common known as Monte Carlo simulation and we drew inspiration from other engineering applications in structural engineering (Beck 2006). Monte Carlo simulation is the simplest method to obtain results from a SFE framework. In a nutshell, the method takes in parameter values from Gaussian distribution and performs finite element analysis to give an output which in our purpose is a 2D temperature map of RF ablation. This simulation is repeated for a certain number of samples which leads to a population of results. The estimates of the output mean and variance is given by

$$E(T_i) = \frac{1}{N}\sum_{j=1}^{N} T_i(j)\,, \tag{5.6}$$

and

$$\sigma^2(T_i) = \frac{1}{N-1}\left[\sum_{j=1}^{N} {T_i}^2(j) - N \cdot E^2(T_i)\right] \quad (5.7).$$

N is the size of population which represents the total number of simulation. The subscript $j$represents the sample number, ranging from 1 to N and subscript i represents the position of the area of concern. Stefanou (2009) noted that a small number of samples (N~50) is only sufficient as a rough approximation of the actual output while a large sample (N~500) is possible to estimate the cumulative distribution function of the output.

Figure 5.1(a) illustrates the cytotoxic temperature area distribution output of a 500 iterations SFE modeling. It is evident that a peak is present in the output similar to the normally distributed parameter inputs. Drawing reference to statistical theory Central Limit Theorem, the close approximation of a normal distribution is viable when sample simulation size gets large. The proposed method is hence statistical in nature and does not give a single solution. However, the method is simplified for our proposed purpose to a look up table method for each simulation. The reason is due to the excessive amount of computational time required if such large number of iterations were to be done for each RF ablation zone.

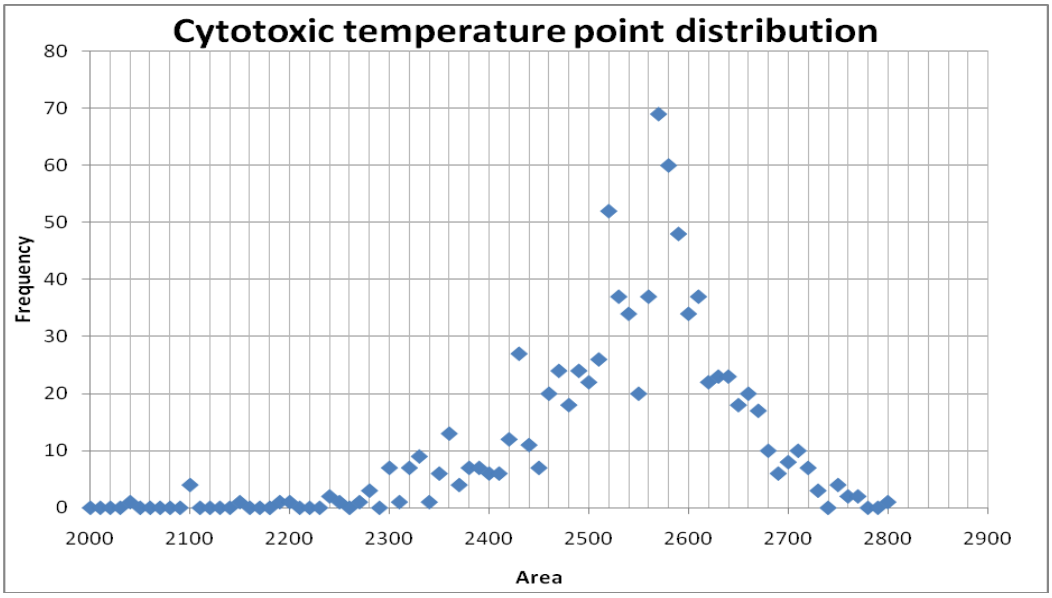

(a)

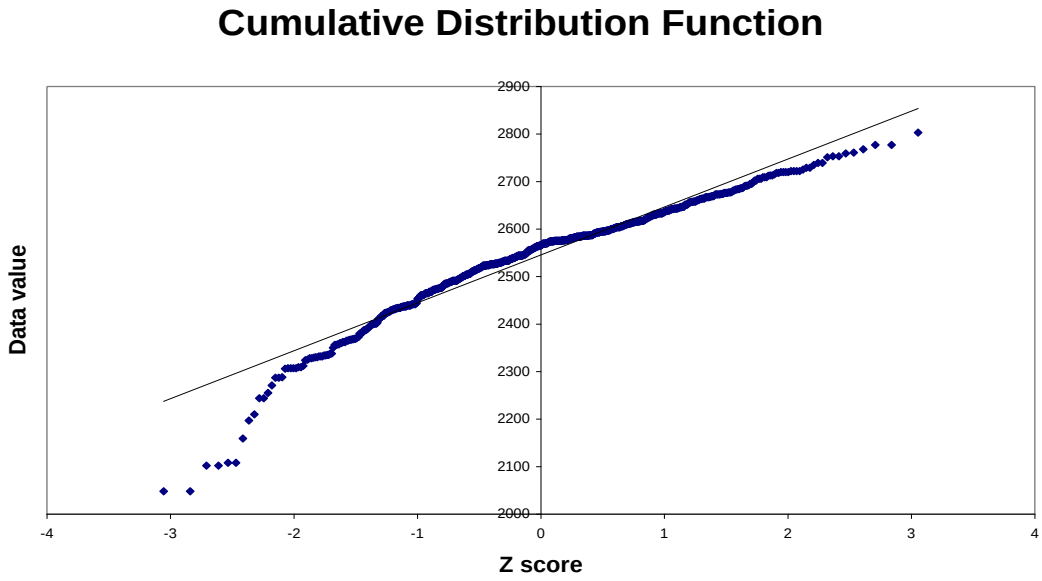

(b)

Figure 5.1. Distribution of tissue area exceeding cytotic temperature (a) Test for normality (b) Results from Stochastic Finite Element Analysis.

We did a test for normality by calculating the area under the Cumulative Distribution Function (CDF) and plotting the Z scores of each data point against its value. A normally distributed data will exhibit a trend line close to a linear line. Figure 5.1(b) exhibits piecewise linear points for a majority of the data points with some discrepancies at the upper and lower value points. This observation will be corrected when the number of simulations increases. Drawing reference to statistical theory Central Limit Theorem (CLT), the close approximation of a normal distribution is viable when sample simulation size gets large. The near normality in simulation result confirms CLT and enabled offline simulation results to be used in RFA planning in the later section.

Tissue properties required for simulation are density, specific heat capacity, thermal conductivity and electrical conductivity. A normally distributed probability density curve for each physical parameter was constructed by taking the mean value from literature and standard deviation assigned to be 10% of the mean value to account for variations. Tissue blood perfusion properties such as blood temperature, blood volume and blood density are not randomized but assigned a value corresponding to the target tissue area perfusion state. For every RF ablation simulation, various physical parameter values were randomly selected from their individual probability density curve and used for the finite element simulation.

RITA Habib 4x Bi-Polar RF probe was used as the electrode geometry. The probe has four electrodes, each 1cm apart and has opposite polarity on each side. During application, the Habib 4x probe makes direct contact with liver tissue and penetrates tissue creating cubic shaped ablation zones. Finite Element analysis was first done for the electric field distribution for Bi-Polar RF ablation by solving the Laplace equation with

geometry electrode dimension modeled as. The Laplace equation was solved in COMSOL and Matlab on a 6cm by 6cm grid, with Dirichlet boundary condition of zero electric field. The voltage used for the Bi-Polar RFA was set at 50V and -50V. The resulting Electric field is available in Figure 5.2(a). It is evident that the electric field is strongest at the electrode interface while it slowly diminishes with distance.

The electric field data is fed into the modified Penne's bioheat equation (Haemmerich 2001) to simulate RF ablation also using COMSOL. The resulting electric field and temperature distribution is available in Figure 5.2. Numerous (up to 500) simulations were ran in a loop with distributed input parameters and results. Typically, cytotoxic temperatures for tumor cell necrosis occurs at 45^{o}C (Stippel 2004) when held for long duration (hours) and within minutes when temperature is above 60^{o}C (Haemmerich 2001, Chang 2004). Hence, a threshold cytotoxic temperature of 50^{o}C is used to quantify tumor cell death. This threshold is easily alterable and can be implemented with a stochastic nature. However, the threshold was decided to be deterministic to simplify the method and for better consistency in results.

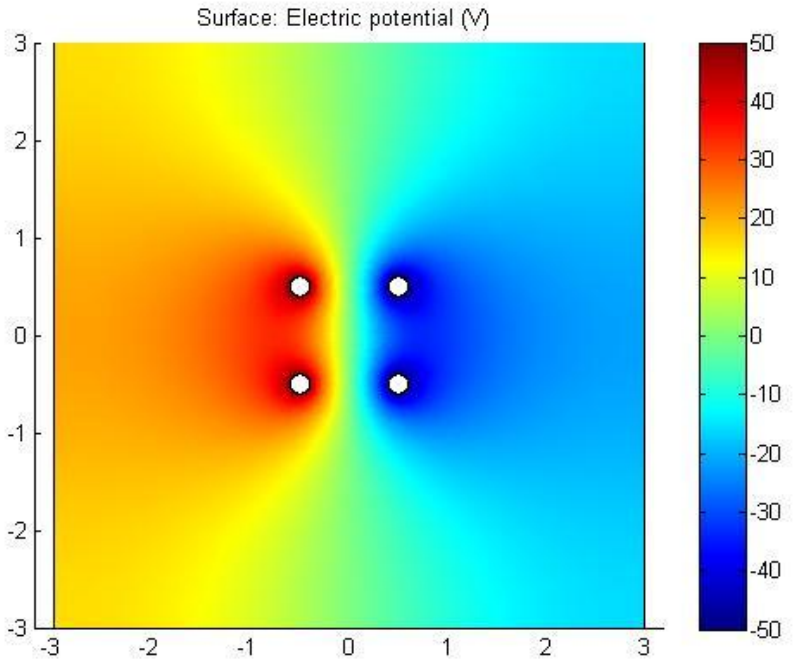

(a)

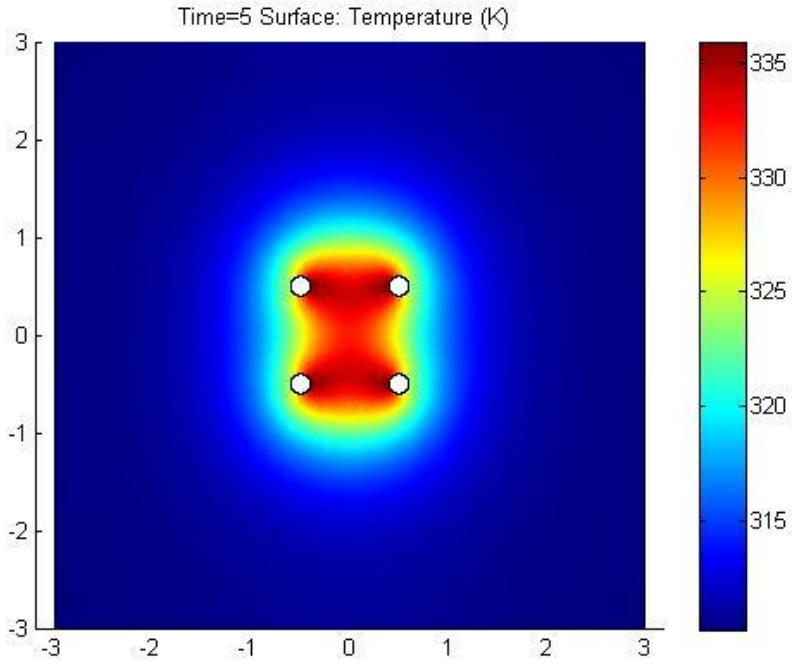

(b)

Figure 5.2. Results from FEM (a) Electric field and (b) Temperature field due to Bi-polar RF ablation

5.4 Surgical planning for tumor ablation

The RFA planning system described in this section is for tumors which are suitable for RFA therapy. Ablation of single small or large tumor, multiple small tumors and large tumors could be planned using the proposed planning system. Single small tumor usually requires a single (or few) RFA application. It is therefore beneficial to plan for optimal placement of probe for complete tumor destruction. The same applies to multiple small tumors which is analogous to several single small tumors. This planning system is applicable to large tumor RF (diameter 8-10cm and above) where many RFA applications are required for full tumor coverage. RFA planning for large tumor is often more complicated due to the existence of blood vessels and the different perfusion state within the tumor.

The RFA planning system is illustrated in Figure 5.3. Offline SFE Analysis is done for 10 perfusion rates which is within the range for normal liver organ. For each perfusion rate, 800 iterations of simulation were done resulting in a distribution of output. For every iteration, the material properties for solving the Laplace and Penne's bioheat equation were selected randomly from a normal distribution similar to described in previous section. Due to the normality nature of the distribution, offline simulation results can be used for online surgical planning. The offline results will enable fast surgical planning during actual surgical planning.

During actual planning, medical imaging technique such as CT scan or MRI is used to capture the area(s) of therapy. The images are processed in an image segmentation algorithm to identify the tumor and the vasculature information. Tumor boundary of 1cm is included into the tumor area during the image

For illustration, a large tumor of size 8-10cm was generated on a 2D grid. The tumor was generated with a random geometry which exhibited angiogenesis nature; blood vessel formation found near the tumor. The method for tumor generation was implemented using Matlab. A random 2D map (20cm by 20cm) was generated and a 8-10cm tumor was formed in the centre by an iterative clustering process. Thereafter, blood vessels were generated in the map with higher probability assigned to the tumor zone. The process of generating angiogenesis was similar to that of percolation theory often used in fractal geometry (Figure 5.3). Angiogenic nature of tumors increases heat sink effect and reduces the effectiveness of RFA. The inclusion of heat sink effect for FE simulation permits more accurate simulation results.

Prior to the start of the RF ablation planning, iterative simulations were done as described in earlier section with a range of blood flow parameters (10 blood flow). This enabled us to select the closest output for a given blood flow perfusion data for the RF ablation zone selected for simulation. This was done to reduce computational time required for large number of iterations for each RF ablation zone.

The first step to our proposed surgical planning was to include a 1cm ablation margin to the tumor in prevention of tumor recurrence (Tranberg 2004, Ni 2005). The target RF ablation region was located by an algorithm and sub divided into squares of 1cm by 1cm which coincided with the Habib 4x probe size. The sub division of the target zone was done to quantify blood flow. Surgical simulation began from the arbitrarily chosen area (bottom left corner) of the target tumor area (Grey box, Figure 5.4). The start position does not affect the accuracy of the simulation however; it will result in a

different final result. This is within expectation as the main purpose of the simulation is to ensure full cancerous cell necrosis.

The physical parameters required for simulation were selected from their respective probability density curve. The perfusion state of the area was summed and a look up table method was used in obtaining the temperature distribution output with the closest matching physical parameters from prior simulations. The planning system described (Figure 5.3) earlier was performed in simulation.

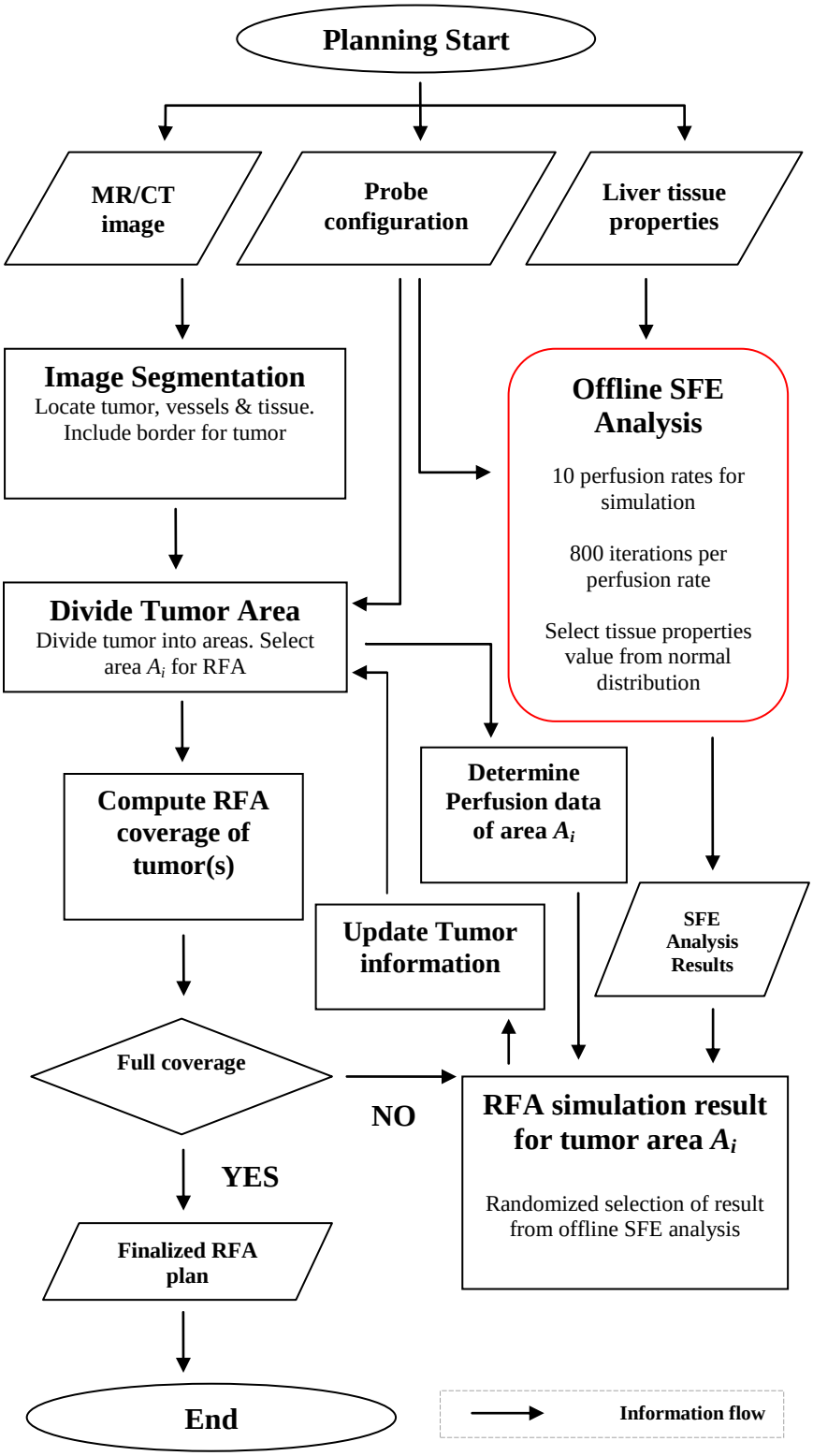

Figure 5.3. Flow chart of RFA planning system

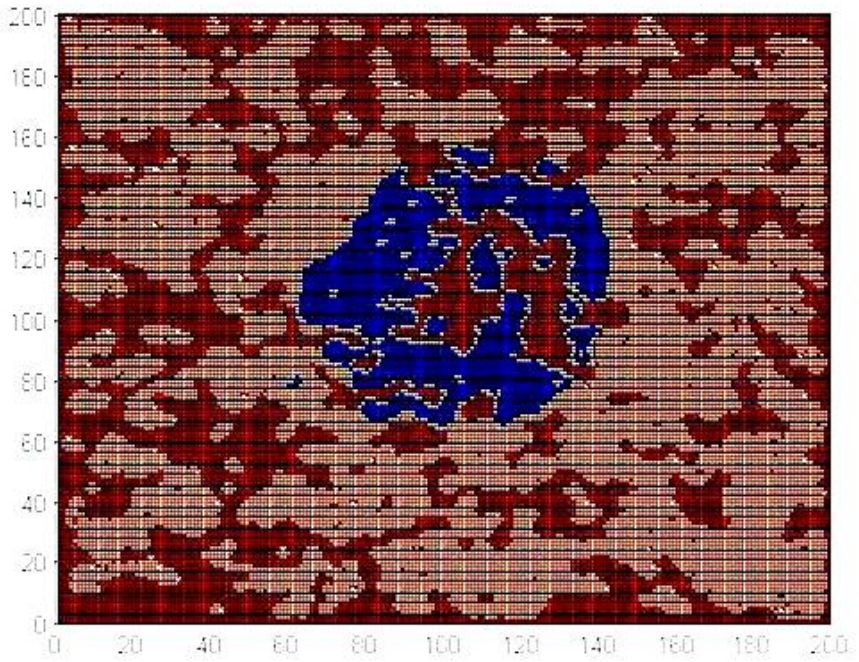

(a)

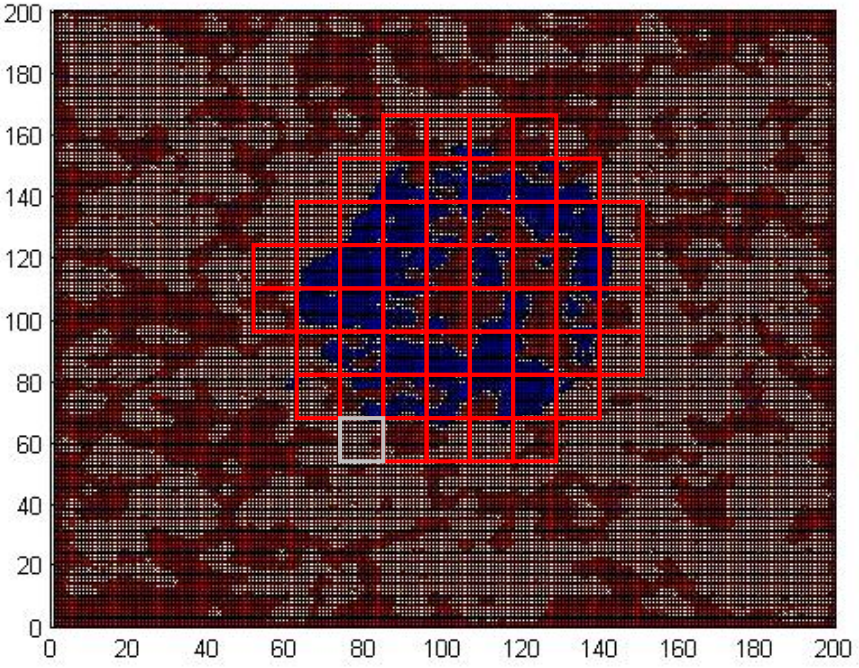

(b)

Figure 5.4. (a) Tumor generated: Tumor (blue), vessels (red) & tissue (pink) and (b) Tumor subdivision with 1cm margin

5.5 Results and discussions

Simulation result for the RFA planning is presented in Figure 5.5. The entire tumor is encompassed by a temperature distribution which is above the cellular threshold. The ablation region includes the tumor margin and alleviates risk of tumor recurrences. With the proposed method, it is easier for surgeons to visualize the placement of RF probes minimizing redundant injury to healthy tissue.

The proposed method demonstrates the feasibility and application of SFE method. It provides a new method for large tumor ablation surgical planning which involves physical simulation and statistics. SFE methods prove to be advantageous compared to existing RF ablation simulations due to the presence of variation, which exists in actual liver tissue. With the inclusion of probability, the method in surgical planning is not purely deterministic. While no actual quantitative studies were done, when analyzed qualitatively the proposed method is more realistic in solving for electric field distribution and temperature distribution. In addition, the method enables multiple solution to be generated and hence a probability based surgical plan. This removes the need for deterministic surgical planning method which might contain intrinsic risks. It enables a more precise and accurate RF ablation planning by surgeons or medical robots.

A limitation to the proposed method is that the method is demonstrated in 2D instead of 3D. While tumors are 3D in shape, a more complicated 3D surgical planning were put on hold in bid to examine the feasibility of this method. We propose the method to be used for large, near planar shaped tumors which are located close to the liver surface. 3D Finite Element Analysis requires much more computational power and time. Blood perfusion data was assumed to be of a single value in the 1cm by 1cm segmented

area. This enables the simulation to account for heat sink effect during RF ablation. A possible inaccuracy in simulation is the lack of relationship between blood volume and the corresponding change in physical properties such as thermal conductivity and electric conductivity.

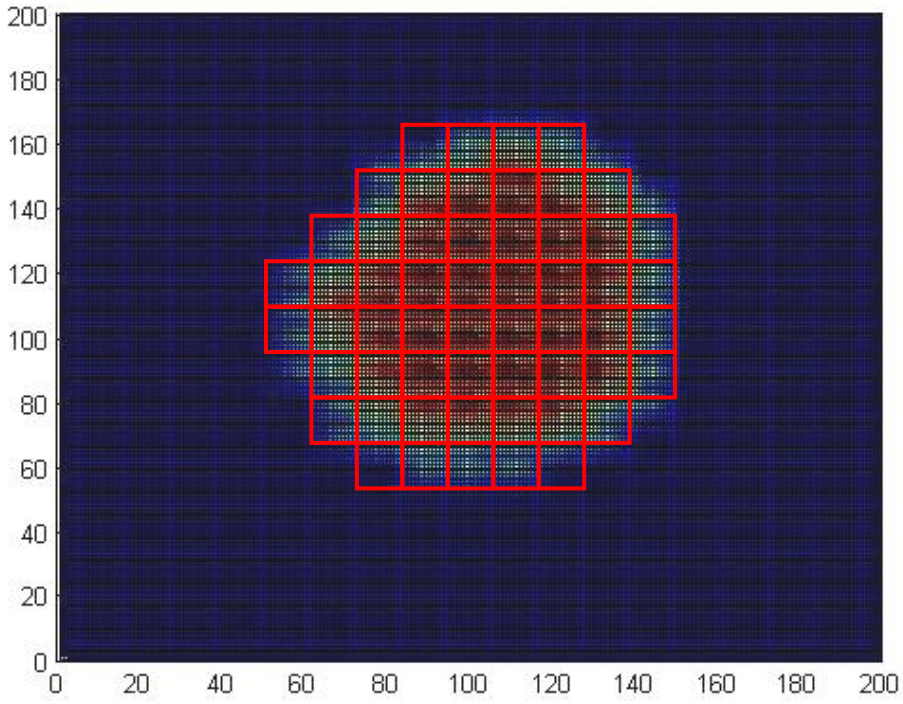

Figure 5.5. Temperature distribution for large tumor surgical planning

A lookup table method was used instead of online iterative simulations which reduced the accuracy of the simulation. The lookup table method draws result from a pool of simulated output which was done offline. This enabled a faster computational time in surgical planning while retaining the stochastic nature of the method. The method does not affect the outcome as the offline outputs were of identical stochastic nature, and draws parameters from the same parametric distribution function.

Evaluation of the efficiency of the proposed system can be done with an in-vitro experiment or animal experiment. For the in-vitro experiment, a blood circulatory system

can be connected to the harvested liver organ to mimic vasculature flow in actual condition. Medical imaging techniques should be used for both in-vitro and animal experiment. The evaluation of the system can be performed by a comparison between user without the planning system to one with the aid of the system. The performances indices are minimum number of ablation applied, minimum overlapping zone and minimum area of healthy tissue destruction.

The proposed method provides good visual illustration with each ablation point accurately transferable to surgical robot for robot assisted surgery (Yang 2010), or presented graphically to the surgeon when incorporated into a medical image processing system for surgical planning. Existing robotic surgery work related to liver ablation [29] by the research team assumes a constant ablation area regardless of variation in physical properties and differing perfusion rate. It does not have a feedback mechanism for planning as all ablation zones are assumed to have identical area or volume. The proposed planning system can make a significant impact by improving the accuracy of ablation planning system. In addition, the system can be expanded by incorporating real time surgical information as feedback for more accurate simulation and planning. The system will devise a surgical plan prior to surgery, and will constantly update itself from an online feedback mechanism during surgery. This feedback loop updates the state of ablation in the area of concern in terms of temperature and tissue cell death which allows the system to fine tune its parameters. Machine learning algorithms can also be deployed for improved surgical planning after each surgery. This capability is advantageous for impromptu deviation from original plans due to factors such as surgical complications.

Chapter 6

INTEGRATED DEVICE FOR ABLATION, BLOOD SENSING AND DIVISION

Chang S KY, Hlaing WW, Huang WH, Chui CK, 2011. Integrated ablation and division device for liver resection. HPB, 13(3).

This chapter contains work from the above cited journal paper which was published in 2011. This chapter describes the design process of a surgical device which is able to perform hepatectomy laparoscopically. The device has an integrated RF ablation needle, laser blood flow sensor and knife blade for resection. Related work to the design of the device was submitted for review to the ASME Journal of Medical Device. Section 1 describes the surgical procedure of Hepatectomy, Habib method and various tissue division methods. Section 2 describes the integrated device and its design principles. Section 3 gives the results from experiments and the concluding section discusses the chapter.

6.1 Hepatectomy and tissue division methods

Radio-frequency assisted methods are widely used in liver cancer treatments. Radio-frequency (RF) pulses (500 KHz) are used to induce ionic agitation and Joule heating, hence coagulation to the liver tissue and cancerous cells (Haemmerich 2004). Hepatectomy refers to the surgical procedure that removes partial liver tissue, which

encapsulates the tumor, from the liver organ. These two processes are often performed separately. A new technique in liver resection was developed by Habib (2006) to maximize the benefit of RF ablation for liver resection procedure with significant reduction in blood losses. Blood losses are associated with increased risk of postoperative complications and hence undesirable (Jarnagin 2002). The RF ablation was first performed on the desired line of resection followed by a manual resection with surgical scalpel. RF energy induces frictional heating causing coagulation for reducing blood loss while cutting.

This new technique combines the advantage of a reduction of blood loss and turmoricidal effect at the resection site without the use of sutures, surgical knots, clips, or glue. There are several advantages to the Habib technique in addition to blood loss reduction. The technique can be easily performed by a surgeon with good knowledge of liver anatomy. The technique also results in reduction of the length of the anesthetic time and the operating time. To achieve the effect of coagulation in normal liver parenchyma is much faster than that in tumor tissue.

Coagulative necrosis in liver tumor tissue takes about 20 min for one probe application, but only 40s to coagulate the same amount of normal liver tissue hence making the procedure very fast. The technique eliminates the need for intensive care unit facilities, and reduces the need to employ Pringle's maneuver (Milicevic 2008) which is often used for conventional tumor ablation for effective RF heating but results in ischemia-reperfusion hepatocellular injury. Ultimately, the technique results in less postoperative mortality and morbidity.

However, there are some limitations to Habib's technique. Firstly, Radio-

Frequency energy should be applied carefully near the hilum or the vena cava because of its potential damaging effect on these structures. Secondly, healthy parenchymal tissue will be sacrificed for the resection procedure. Thirdly, it is not possible for the surgeon to be sure of the complete coagulation of the tissue along the cutting plane. Hence, occasional blood losses will be encountered during operation. This is evident in one of the cases done by clinical teams and we will be offering a solution to this.

Several medical trials were done by many medical teams using the same technique. Dr Habib and his team performed the technique on a 69-year-old gentleman with colorectal liver metastases whom underwent a segment II/III liver resection following preoperative staging with spiral computed tomography (CT) scan. The segmental resection was then carried out according to the technique described above. The resection time was 45 min with a total blood loss of 30 ml during the division of the liver parenchyma. There was no morbidity in the patient and excellent recovery was observed in the patient who was discharged after 5 days.

Pellici (2006) conducted clinical trials on 17 patients (8 women and 9 men with mean age of 72years old.) who underwent Radio-frequency assisted liver surgery. Seven patients were affected by hepatocellular carcinoma; the other nine had colorectal liver metastases and one case with gastric metastases. There were no operative deaths from all 17 patients. Mean operative time was 220 min (ranging from 110 to 420 min). Mean blood loss was a very optimistic value of 53 ml (ranging from 5–150 ml) with no further devices involved (stitches, clips, tissue glue, and argon beam coagulator) but Radio-frequency energy was required, to get adequate hemostasis. No patient received blood transfusion and Pringle maneuver was never required. One patient had an important

intraoperative bleeding (total blood loss 150 ml) from an incompletely coagulated blood vessel, which was managed with manual compression and further RF sessions.

We report a surgical device and method that incorporates both RF ablation and hepatectomy procedures. A Laser Doppler Flow (LDF) sensor was embedded in the device for blood flow sensing to firstly, ensure minimal blood flow prior to resection, and secondly, prevent excessive tissue ablation. A user interface, which displays LDF sensor data graphically, provides the surgeon with real time blood flow readings from the flow meter, and visual and audio signals when the ablated tissue is ready for resection. Finite Element simulations were used to justify design parameters of Radio-frequency electrode placement.

In vitro experiments were conducted on in-vitro porcine liver model with a simulated fluid circulatory system attached to the portal vein for simulating blood perfusion. In-vivo experiments were performed on live porcine models in laparoscopic setting to measure the reduction in blood losses and efficiency of the device.

6.2 Integrated device prototype

6.2.1 Overview

A device (Figure 6.1.a) was built to perform the Habib's technique in a single device, combining both procedures of radio-frequency ablation and hepatectomy. The prototype enables a laparoscopic surgical procedure and removes the need for switching of tools during surgery. A Laser Doppler Flow (LDF) Sensor was integrated for blood flow detection prior to cutting. The LDF sensor ensures minimal blood flow in the target tissue and prevents unnecessary blood losses during resection. The sensor is connected to

a computer via a data acquisition card and presents real time graphical information to the user.

A few design parameters were specified for the device. The device has to be small in diameter (15mm) and long (30cm) for laparoscopic surgery. A biocompatible material is required in preventing biological host response and thus plausible complications during surgery. Modular design was employed for the prototype which consists of detachable components to ease the replacement of device parts. Components which have a constant inner diameter for connection are held down by set screws. This design allows efficient replacement of faulty or soiled parts for fast turnover time between servicing.

Figure 6.1.a Tissue ablation and division prototype device

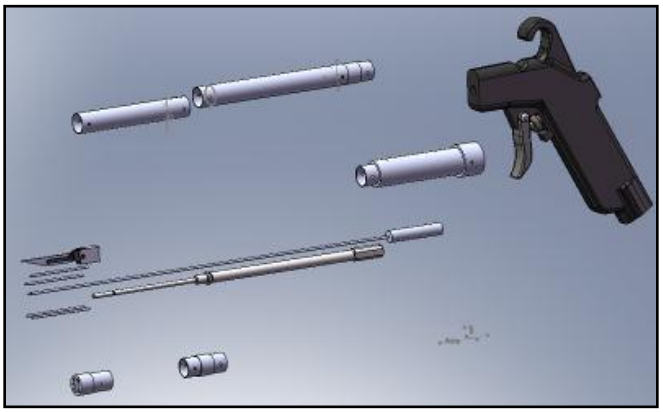

Figure 6.1.b. Modular design of the prototype device.

6.2.2 Material selection and prototype design

The two biocompatible materials selected for direct contact with the liver tissue are Delrin and 304 stainless steel. Delrin, also known as Polyoxymethylene, (POM) is an engineering thermoplastic plastic approved by US Food and Drug Administration (FDA) for surgical use. This light weight material, which has good wear and high temperature resistances,, is suitable for use at the distal end of the device that contacts the tissue. Type 304 (AISI) stainless steel was selected for the construction of the prototype body (Figure 6.1.b). Type 300 series are austenitic chromium-nickel alloys that consist of lower carbon content to ease forming. The 18/8 stainless steel contains around 18wt% Chromium and 8wt% Nickel has generally good resistance to corrosive environment. The resistance is improved by increasing the Nickel and Chromium content. Austenitic steels are prone to corrosion especially with the presence of chloride ions. Steel corrosion is reduced with high nickel austenitic alloys.

The design of connective steel lube is not trivial due to the multiple components within. Design for assembly was done to effectively assemble all the parts without causing damage to individual components. The size of the parts increases the difficulty in assembly hence design for assembly greatly helps in the assembly process.

6.2.3 Prototype assembly

The device was assembled into an integrated device with the three main functions: Ablation, resection and blood flow sensing. Figure 6.2 shows a CAD 3D model of the device with various parts integrated into the laparoscopic device. A handle is attached to the prototype which has a switch to toggle pneumatic valve for knife blade actuation.

Sections of the tube were assembled with interference fitting as fasteners were deemed unsuitable due to their protrusion from tube surface. Interference fit also allows quick disassembly for part changes and maintenance. The Laser Doppler Sensor was mounted at the tip of the device with a rubber O-ring keeping it in position and providing protection. A retractable knife blade mechanism is attached to the foremost tube via a tapped screw thread. The knife blade will perform the resection in the ablation zone.

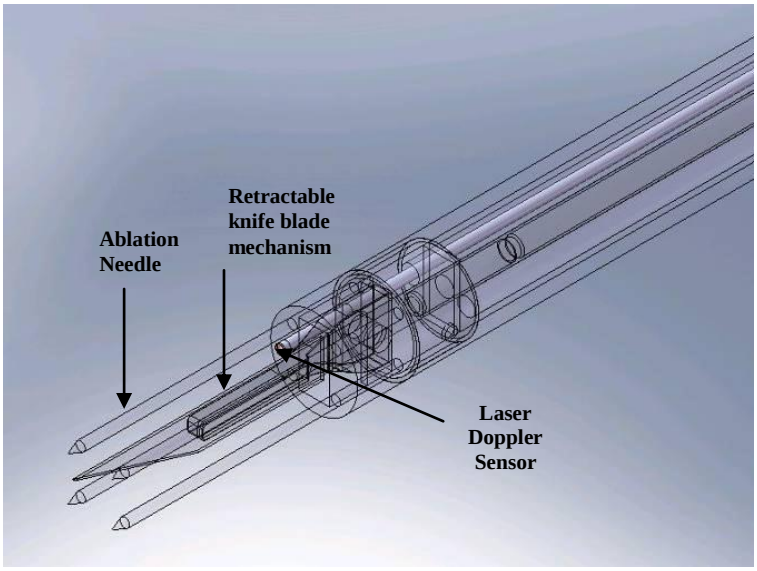

Figure 6.2. Position of various parts

6.2.4 Ablation mechanism and optimal electrode placement

Gold plated ablation needles were removed from existing Habib 4x bipolar probe and fitted onto the prototype. Each ablation needle plated to reduce surface current formation and the sharp tip ensures minimal deformation prior to tissue break point. The ablation needles were connected to the Rita 1500X RF Generator, a 100W rated generator and was set to an impedance-controlled mode during usage. Impedance controlled mode controls and stops the ablation process by sensing tissue impedance in between the RF needles.

Figure 6.3(a) and 6.3(b) present the temperature distribution from finite element analysis for 4-electrodes and 2-electrodes arrangement. The simulation was done to investigate the optimum number of bipolar electrodes to be used and their polarity placement. Comsol Multiphysics 4.1 was used to simulate the electric currents between the needles and thus the temperature distribution due to RF ablation. The finite element analysis was performed as follows. Material properties were input into the program and an electric field was simulated according to the location of ablation needles and the electric power applied. The electric field generates heat in the tissue especially near the ablation needles and hence heat transfer to the other parts of the tissue. The Joule bioheat equation was then used to simulate the temperature distribution of the tissue and its response in time. This gives us an understanding of how the burning zone will develop and aid in our placement of electrodes.

Referring to the figure 6.3(a), the two circles on the left represent positively charged electrodes while the two on the right represent negatively charges electrodes. It can be observed that the zone of maximum temperature is between the needles and the plane perpendicular to it. This is highly desirable as it coincides with the cutting plane. This is will make sure that the cutting plane is experiencing the highest temperature and hence lower risk of blood flow. Higher temperature will result in higher probability of coagulation of blood. Taking into account the variability of tissue properties, a probability based finite element method was used to estimate the temperature distribution. A general pattern of a vertical high temperature plane was observed.

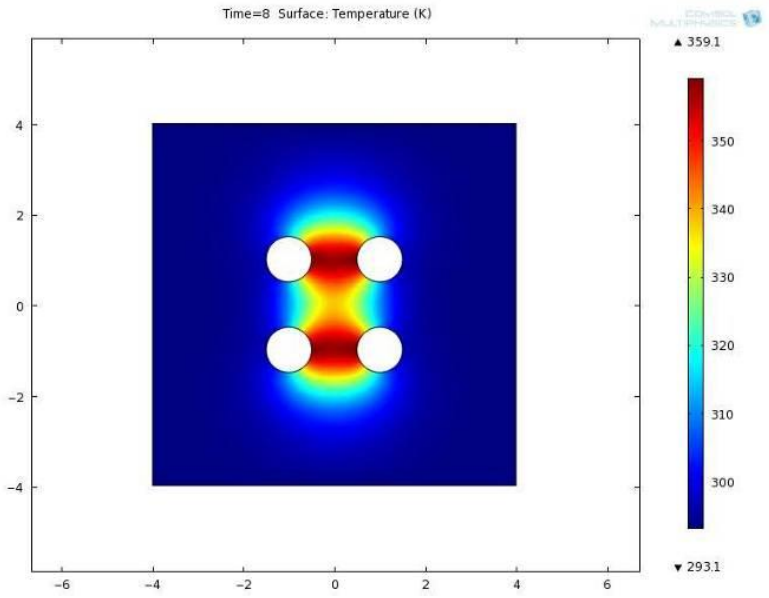

(a)

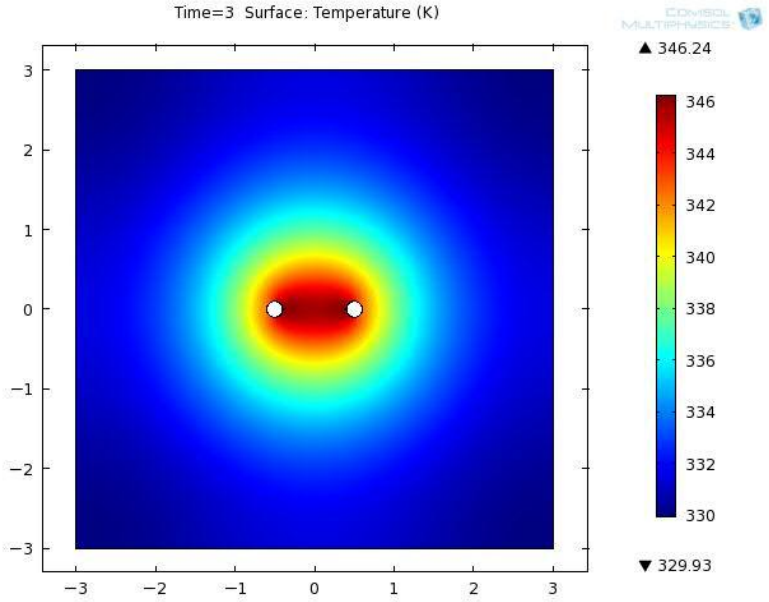

(b)

Figure 6.3. Finite Element Results. (a) Temperature distribution for 4-electrodes RF ablation. (b) Temperature distribution for 2-electrodes RF ablation.

6.2.5 Blood flow detection

Almond (1992) investigated the performance of LDF with changes in flow characteristics in the hepatic microcirculation. Red blood cell (RBC) flux measured by LDF sensor is sensitive to alterations in red blood cell velocity and concentration. It was concluded that the value of continuous real-time monitoring without perturbation of circulation is extremely valuable compared to other techniques. LDF sensor incorporates such advantages and hence is preferred to other blood flow monitoring technologies. The reliability, non-invasiveness and simplicity of LDF application are also major advantages. In addition, small dimensions of the probe also make it suitable for our application, to be integrated into a laparoscopic device.

MoorVMS-LDF2 Laser Doppler Blood flow Meter (Moor Instruments 2009) from Moor Instruments was selected for the integrated LDF. The meter has a dual channel input, for two LDF optical fiber sensors to be used at any one time. The LDF optical fiber sensor is 1.5mm in diameter with a sensing volume of 5mm in radius. Sensor outputs low power monochromatic laser which is safe without the need for additional protective kit. The sensor is able to sense capillary diameter of 10microns with a flow spectrum of between 0.01 to 10 mm/s. The sensor is placed adjacent to the knife blade for blood flow detection in the cutting plane.

A data acquisition card was used to collect real time data from the Laser Doppler Blood flow Meter and a computer user interface was built using Labview 8.6 (Figure 6.4). Real time data is presented to the surgeon with a graphical plot of the Flux and the DC value. Flux value represents the Red blood cell velocity and concentration while the DC value represents the intensity of reflected laser beam. The DC was found to be able to distinguish between surfaces of different color due to the different amount of laser

adsorption for each color. Hence, the DC value was used as a second confirmation of a well ablated tissue.

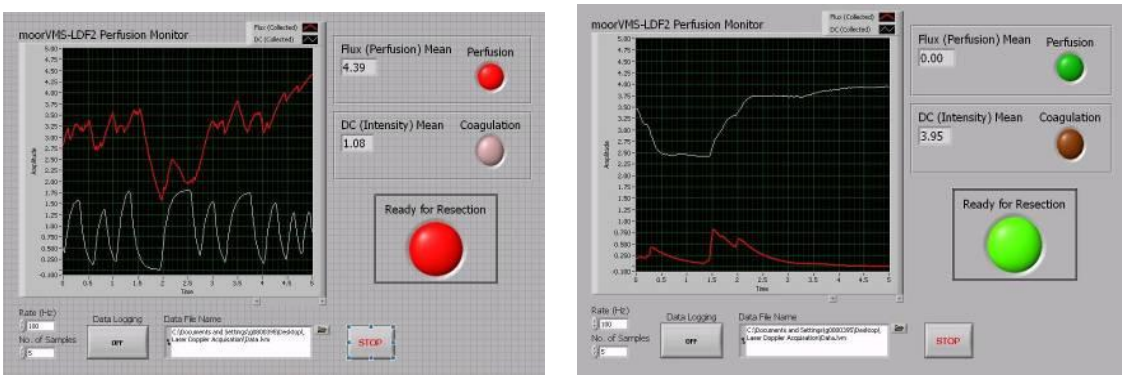

Figure 6.4. User interface for LDF information display

Prior to integration of sensor, experiments were done to calibrate the sensor and relate it to fluid flow velocity. This helps surgeon to better visualize blood flow in terms of velocity instead of the more unconventional flux unit. In addition, it'll help us to decide on a value as benchmark for interface to decide if a resection action should be performed.

The experiment was performed using a PH800 Dymax aquarium pump which was connected to a 0.25inch valve and the outlet pressure measured with a pressure gauge. Fluids used for calibration were water (less viscous) and milk (viscosity closer to blood) pumped through a thin transparent polymer pipe of 3mm diameter. The LDF sensor was mounted to sense for Flux and DC readings with different flow velocity. Results for both water and milk were recorded and plotted (Figure 6.5(a) & Figure 6.5(b)).

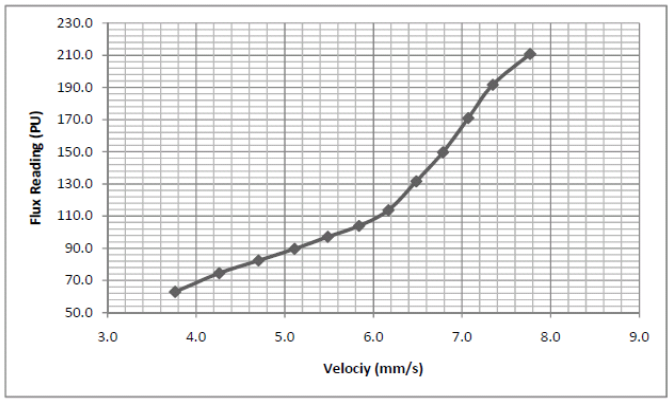

(a)

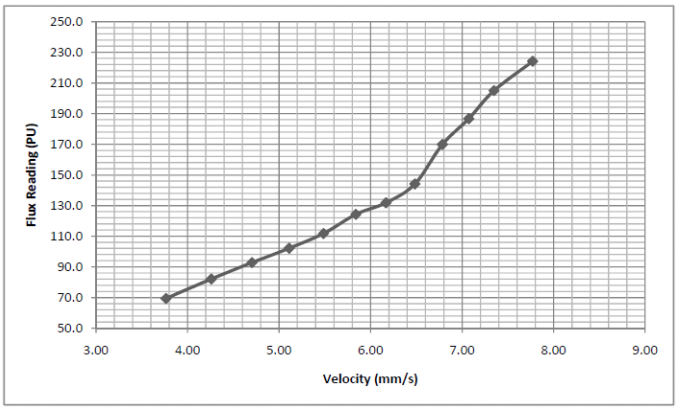

(b)

Figure 6.5. (a) Calibration of LDF Sensor with water (b) Calibration of LDF sensor with milk

Results obtained in both cases shows piece-wise linear behavior between flow velocity and flux values. Piece-wise linear curves can be explained due to pipe wall resistance and varying fluid boundary layer with different velocities. It was observed that slope of curve for milk is steeper compared to that of water due to higher viscosity.

Comparison with results obtained by Almond et al done on rats hepatic perfusion of varying concentration showed consistency in relationship between viscosity and steepness of curve. Hence, the calibration results can be used as a preliminary guideline for the LDF sensor integrated and will aid in more accurate calibration during in vivo studies.

6.2.6 Resection mechanism

Pneumatic cylinder actuator from SMC, CDJ2B6-60SR-B, was identified as suitable for our usage. It is a single acting spring return air cylinder. The cutting blade was mounted onto the air cylinder with a blade holder. A pneumatic valve was connected to the air cylinder for the control of the actuation stroke while the return stroke is spring actuated. Pneumatic actuation was chosen as it provides the fastest actuation speed at the smallest possible size. Other alternatives such as electromagnetic actuators, spring loaded actuators and motor driven actuators were explored and concluded to be unsuitable. A pistol handle was integrated for optimal comfort for the user with knife blade actuation lever mounted on it.

Experiments were conducted to investigate the effects of blade shape and thickness on cutting. Several different blades were tested; ranging from surgical blades to self-fabricated and sharpened blades. Feedback from medical staff suggests that knife cut opening visibility is an important issue during surgery as it will facilitate placement of the device for the next cut. Tests were done on a mechanical loading setup to investigate the force required for ablated tissue penetration. Surgical blades require the least force for penetration while self-fabricated square blades require three times the force required for penetration.

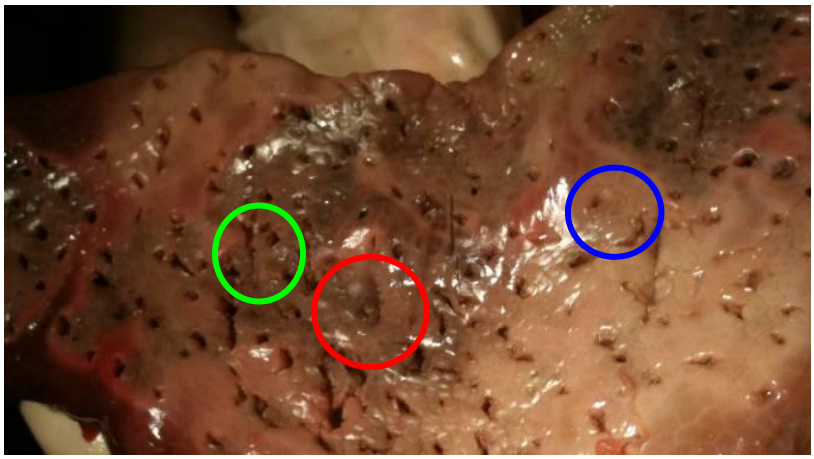

Figure 6.6. Knife blade visibility. (L to R) Small square blade, large surgical blade, large square blade

The image showing the various cuts are available in Figure 6.6. It is evident that the square blades (in green and red circle) give more visible cuts to the ablated liver tissue. The surgical blade which requires less force, gives a cut with very low visibility. The square blade was chosen to be more suitable due to its better cut visibility. Cutting force is of least importance as we are able to provide it in abundance from the pneumatic actuator.

6.3 Experiments

6.3.1 In-vitro experiments

In-vitro experiments were conducted with a liver harvested from the abattoir. An external circulation system was used to mimic the flow of blood through the liver. The circulator system comprised a fluid pump to ensure fluid circulation through the liver test sample via the hepatic portal vein. This enables flow in the vessel of the liver specimen to better reproduce actual in-vivo conditions. However, the fluid is a mixture of blood and water of a lower temperature as compared to actual blood at body temperature. Naturally

occurring blood coagulation was not replicable during the device testing. Results from the device testing were satisfactory as the device was able to produce good resection with minimal fluid loss was achieved. However no actual fluid loss was measured due to the motivation of the test was a functionality test compared to a performance test. The in-vitro setup lacks the actual laparoscopic environment, elements of space constraint, a pressurized interior and actual physiological condition.

6.3.2 In-vivo experiments

Animal experiment was conducted to test the new device (Chang 2011). The experiment was conducted in compliance to the National Advisory Committee for Laboratory Animal Research of Singapore as well as IACUC guidelines. All animals tested underwent approved procedure and protocols in minimizing pain and discomfort. The experiment was conducted in Advance Surgical Training Centre (ASTC), National University Hospital of Singapore. The facility has state-of-the-art surgical setup for testing surgical devices (Figure 7). Comparative study with conventional devices was performed. A left lateral liver resection was performed on a 45-kg live adult pig using the described device and a similar procedure was performed on another porcine model using a commercially available device. A Computed Tomography (CT) opaque dye gel was injected to simulate a tumor in the liver. Intraoperative blood loss and duration of resection were compared. The new device took a total of 20 minutes for the resection with a blood loss of 100ml while the commercial device took 25 minutes with a blood loss of 150ml. Results were encouraging as the prototype managed to perform its intended task by completing the surgery in the intended time. Although the results were based on a single test, it was encouraging for the proof of concept of the device.

6.4 Discussion

This chapter reports the design, development and evaluation of a new surgical device for hepatectomy. An effort was made to incorporate the Habib method of liver resection, using Radio-frequency ablation for hepatectomy, into a single device. A blood sensing Laser Doppler sensor was also integrated for confirmation of blood flow stoppage. Several design parameters were reviewed and computer simulation was employed for better device design. Design process involves material selection for the device body, part design for mechanisms and mountings, components selection for actuator and sensors, and finally design for assembly for all the parts. Computer simulation using finite element was used to refine the design for radio-frequency electrode placement. Device testing was done in-vitro on a liver sample with a fluid circulatory system connected. Good results from the device were achieved. In-vivo animal experiment was conducted on two live porcine models comparing the new device to existing devices available in the market. Result from the new device was satisfactory as it met the target for the surgical time while minimizing blood losses.

Chapter 7

CONCLUSION

This chapter outlines the main contributions of this thesis in the field of radio-frequency ablation. Potential directions for future research are also highlighted in the chapter and finally, it includes the concluding remarks for the thesis.

7.1 Contributions

A new bioimpedance dispersion model for soft tissue is proposed. The new model builds upon conventional Debye model which has a sound physiological reasoning and expands it from a single cellular representation into its tissue level. Multi-scale modeling technique was applied to integrate the different size levels. In addition, blood vessels are incorporated into the model as water plays a major role in directing the Gamma dispersion region of soft tissue. The model is physiologically sound and results from the model are compared to classic Cole-Cole model. The comparison shows that the proposed model is able to fit experimental results better than the classic model.

Since 1940s, researchers have published in-vivo human bioimpedance data which are of valuable purpose. However, the work has not been fully understood due to an incomplete understanding of the tissue bioimpedance dispersion. This model contributes to our continue understanding of physical properties of biological tissue. This understanding is part of a continuous effort to model tissue properties in hope of

developing technologies in biomedical field. It was mentioned in previous chapter that the model can be potentially used in the quantification of shifts in bioimpedance dispersion for a new blood sensing technology. The technology will be a minimally invasive way in detecting blood volume within a tissue volume. While the model is not limited exclusively to liver tissue, it is particularly suitable due to the high level of perfusion in the liver organ.

Radio-frequency ablation induces heat in the tissue and thus cellular necrosis which changes the tissue structure and composition. These structural changes are evident from material changes such as tissue color in terms of optical properties, stiffness in terms of mechanical properties and increased impedance for electrical properties. The tissue material properties are altered in an irreversible way due to permanent cellular damages. Work was done on relating mechanical properties to electrical resistance in the process of RF ablation.

A model was built to mimic the bioimpedance changes of tissue due to RF ablation. Various tissue samples undergoing different amount of RF ablation were tested for their mechanical properties. This enables us to understand how mechanical properties change in the course of RF ablation. A general observation was made that the stiffness of tissue samples increase with ablation. However tissue stiffness plateaus to a value with increasing stiffness. This is due to the over compacting of cells at high strain. A 3D graphic representation enables visualization of how RF ablation and tissue mechanical properties change.

Variation is probably the biggest hurdle in biomedical simulation and modeling. The variation can occur within a single test subject as well as between several subjects.

Properties variation is commonplace and the assumption of a homogeneous material is hence invalid. Stochastic finite element modeling is proposed to be incorporated into a tumor RF ablation planning system. The method is statistical in nature and does not reply on the assumption of homogeneous material. The material properties for deterministic methods were represented by Gaussian distributions to account for naturally occurring variations. Although there is no knowledge if such variation is Gaussian by nature, it can be assumed to be Gaussian by Central Limit Theorem (CLT).

The stochastic finite element method was used for surgical planning to better predict RF ablation affected zones, effective cell necrosis area and to ensure a safety margin in prevention of relapses. The novel method is suitable for single small tumor, multiple small tumors and large tumor. It can be used as a guide for surgeons or integrated into a medical robotic system.

A device was built to perform the Habib's method of hepatectomy (liver resection). Finite element analysis was used to study the temperature distribution due to Rita 4x catheter for RF ablation. It was concluded that the mid-plane between the bi-polar pairs of electrode needle experiences the highest temperature. Hence, it could be deduced that it is best suited for the resection plane due to highest probability of blood coagulation and lowest risk of blood losses. Laser Doppler blood flow sensor was integrated in the device for blood sensing. Calibration of the device was done to quantify blood flow and the material opacity of tissue sample. In addition, a study of knife blade geometry was conducted to select the most suitable knife blade design.

7.2 Future work

It was mentioned in previous chapter that a more complete model is required to accurately simulate the RF ablation process. Water evaporation, mass transport and vapor condensation are the few of the many physical processes which occurs in real but are not accounted for in classical models (Jiang 2007). In addition, works on physical properties are needed for RF ablation simulation due to their temperature dependence. It is important to study how physical parameters such as dielectric and thermal properties vary with tissue injury and temperature. While mechanical properties are a function of temperature, Walsh (1989) concluded that it contributes to the effectiveness of hyperthermia treatments. Various RF ablation simulation methods were reviewed in the earlier section. However, a common short-coming is the assumed constant physical properties for all tissue samples. The assumption of constant physical properties in liver sample is inaccurate due to variation in micro structure and micro perfusion. In addition, liver tumors are angiogenic in nature thus altering perfusion state around the tumor. Variations in physical properties such as electrical conductivity, thermal conductivity, perfusion rate and density affect the final output of the simulation and should not be assumed to be identical. Statistical methods can be used to account for the variations in a statistical framework.

The field of relating temperature, tissue injury and mechanical properties, tissue variation remains a hurdle in characterization of the properties. Variations exist on the macro scale between patients, in anatomy of organs or vasculatures and on the micro scale, in cellular variations and bulk tissue properties. The author believes that there is a link between the Mechanical, Electrical and Thermal properties of tissue which can be

characterized from its tissue structure. These properties change in accordance to changes in tissue structure such as undergoing RF ablation.

In conclusion, much work remains to be done to gain more insight into the science of hyperthermia treatment. There were many reports on topics such as simulation temperature distribution, observing histological changes and quantifying mechanical properties, there is a lack of work in relating these topics to fully understand how tissue react to temperature changes. In addition, statistical methods prove to be appropriate in tissue modeling due to innate tissue properties variation. The consideration of differences in properties will further enhance the accuracy of our current simulation and optimize the procedure and devices for best clinical effects.

7.3 Conclusion

Radio-frequency (RF) ablation is commonly used for hepatic carcinoma treatment. RF ablation applies a high frequency (550KHz) voltage to biological tissue generating heat. Understanding the science of ablation is valuable. Quantifying heat transfer for RF ablation is done by solving Penne's bioheat equation. Tissue impedance affects RF ablation effectiveness. A Multi-Scale impedance model was proposed to mimic the bioimpedance of liver tissue. The model outperforms the classic Cole-Cole model while providing sound physiological explanation. The effect of RF ablation was studied and presented in a 3D plot, correlating tissue injury and physical properties. A novel Stochastic Finite Element (SFE) method was proposed for large tumor RF ablation planning to account for tissue variation and clinical limitations. A novel method using RF ablation for blood loss reduction in hepatectomy was integrated into a laparoscopic

device. The device was tested in-vivo on a porcine model with results showing competitiveness with existing products.

REFERENCES

Adam A and Mueller P, 2009. Interventional radiological treatment of liver tumors. Cambridge: Cambridge University Press.

Ahmed M, Liu Z, Humphries S, Goldberg SN, 2008. Computer modeling of the combined effects of perfusion, electrical conductivity, and thermal conductivity on tissue heating patterns in radiofrequency tumor ablation. Int. J. Hyperthermia. 24(7): 577-588.

Almond NE, Wheatley AM, 1992. Measurement of hepatic perfusion in rats by laser Doppler flowmetry. American Physiological Society. 262(2 Pt 1):G203-9.

Argyris J, Papadrakakis M, Stefanou G, 2002. Stochastic finite element analysis of shells, Comput. Methods Appl. Mech. Engrg. 191, 4781–4804.

Arkin H, Xu LX, Holmes KR, 1994. Recent Developments in Modeling Heat Transfer in Blood Perfused Tissue. IEEE Transaction on Biomedical Engineering, 41, 2, 97-107.

Baldwin S, Pelman A, Bert JL, 2001. A Heat Transfer Model of Thermal Balloon Endometrial Ablation. Ann. Biomed. Eng., 29, 1009-1018.

Baroth J, Bodé L, Bressolette PH, Fogli M, 2006. SFE method using Hermite polynomials: an approach for solving nonlinear mechanical problems with uncertain parameters, Comput. Methods Appl. Mech. Engrg. 195, 6479–6501.

Beck AT and Rosa ED, 2006. Structural reliability analysis using deterministic finite element programs. Latin American Journal of Solid and Structures, 3, 197-222.

Bellia SA, Saidane A, Benzohra M, Saiter JM, Hamou A, 2008. Dimensional soft tissue thermal injury analysis using transmission line matrix (TLM) method. Int. J. Numer. Model, 21, 531-549.

Burrage K, Tian T, Burrage P, 2004. A multi-scaled approach for simulating chemical reaction systems. Prog. Biophy. Mol. Bio. 85, 217-234.

Chang IA and Nguyen UD, 2004. Thermal modeling of lesion growth with radiofrequency ablation devices. BioMedical Engineering OnLine. BioMed Central.

Chang S KY, Hlaing WW, Huang WH, Chui CK, 2011. Integrated ablation and division device for liver resection. HPB, 13(3).

Chen MH, Chen MH, Yang W, Yan K, Zou MW, Solbiati L, Liu JB, Dai Y, 2004. Large Liver Tumors: Protocol for Radiofrequency Ablation and Its Clinical Application in 110 Patients – Mathematic Model, Overlapping Mode and Electrode Placement Process. Radiology, 232, 260-271.

Chen MH, Wei Y, Yan K, Gao W, Dai Y, Huo L, Yin SS, Zhang H, Poon RT, 2006. Treatment Strategy to Optimize Radiofrequency Ablation for Liver Malignancies. J Vasc Interv Radiol, 117, 671-683.

Chiew YC and Glandt ED, 1984. Interfacial Surface Area in Dispersions and Porous Media. Journal of Colloid and Interface Science, 99, 86-96.

Chin L, Sherar M, 2000. Changes in dielectric properties of ex vivo bovine liver at 915MHz during heating. Physics in Medicine and Biology, 46, 197-211.

Chui CK, Kobayashi E, Chen X, Hisada T, Sakuma I, 2004. Combined compression and elongation experiments and non-linear modeling of liver tissue for surgical simulation, Medical & Biological Engineering & Computing, 42, 787-798.

Chui CK, Nishimura Y, Kobayashi E, Inada H, Sakuma I, 2002. A Medical Simulation System with Unified Multilevel Biomechanical Model. International Congress on Biological and Medical Engineering.

Clegg ST and Roemer RB, 1993. Reconstruction of Experimental Hyperthermia Temperature Distribution: Application of State and Parameter Estimation. ASME Journal of Biomechanical Engineering, 115, 380-388.

Cole KS and Cole RH, 1941. Dispersion and Adsorption in Dielectrics. Journal of Chemical Physics. Volume 9. 341-351.

Craciunescu O, 1998. Influence of Blood Vessel Networks on Hyperthermia Induced Temperature Distributions. UMI Dissertation Services. PhD Thesis.

Craciunescu O, 1999. Influence of blood vessel networks on hyperthermia induced temperature. UMI Microform 9904030.

Delalleau A, Josse G, Lagarde JM, 2011. Dual-parameter optimization of the elastic properties of skin. Computer Methods in Biomechanics and Biomedical Engineering. Vol. 15, No. 1, 83-92.

Dissado LA, Alison JM, Hill RM, McRae DA, Esrick MA, 1995. Dynamic scaling in the dielectric response of excised EMT-6 tumors undergoing hyperthermia. Phys Med Biol, 40(6), 1067-1084.

Dodd GD, Frank MS, Aribandi M, Chopra S, Chintapalli KN, 2001. Radiofrequency Thermal Ablation: Computer Analysis of the Size of the Thermal Injury Created by Overlapping Ablations. AJR, 177, 777-782.

Dumas JH, Himel HD, Kiser AC, Quint SR, Knisley SB, 2008. Myocardial electrical impedance as predictor of quality of RF-induced linear lesions. Physiological Measurement, 29, 1195-1207.

Esrick MA and McRae DA, 1992. The effect of hyperthermia-induced tissue conductivity changes on electrical impedance temperature mapping. Phys. Med. Biol. 39, 133-144.

Fuentes D, Yung J, Hazle JD, Weinberg JS, Stafford RJ, 2012. Kalman Filtered MR Temperature Imaging for Laser Induced Thermal Therapies. Vol. 31, No. 4, 984-994.

Gabriel S, Lau RW, Gabriel C,1996. The Dielectric properties of biological tissues: III. Parametric models for the dielectric spectrum of tissues. Phys. Med. Biol. , 41, 2271-2293.

Gao F, Niu H, Zhao H, Zhang H, 1998. The forward and inverse models in time-resolved optical tomography imaging and their finite element method solutions. Image and Vision Computing, 16, 703-712.

Gersing Eberhard, 1999. Monitoring Temperature-Induced Changes in Tissue during Hyperthermia by Impedance Methods. Annals New York Academy of Sciences.

Goldberg SN, Gazelle GS, Solbiati L, Rittman WJ, Mueller PR, 1996. Radiofrequency tissue ablation: increased lesion diameter with a perfusion electrode. Acad Radiol, 3, 636-644.

Greenleaf JF and Chen S, 2007. Measurement of mechanical properties of homogeneous tissue with ultrasonically induced shear waves. Medical Imaging, 6513, 65130F-1.

Grimnes SJ and Martinsen ØG, 2005. Cole Electrical Impedance Model – A Critique and an Alternative. IEEE Trans on Biomedical Engineering, 52, 1.

Habib NA, 2006. Radio Frequency Assisted Liver Resection: The Habib's Technique. Liver and Pancreatic Diseases Management, 31-37. Springer

Haemmerich D, Staelin T, Tungjitkusolmun S, Lee J, Mahvi DM, Webster JG, 2001. Hepatic Bipolar Radio-Frequency Ablation Between Separated Multiprong Electrodes. IEEE Transactions on Biomedical Engineering. Vol 48. 10.

Haemmerich D, Chachati L, Wright A, Mahvi D, Lee F,Webster JG, 2003. Hepatic Radiofrequency Ablation with Internally Cooled Probes: Effect of Coolant Temperature on Lesion Size. IEEE Trans. On Biomedical Engineering, 50, 4.

Haemmerich D, 2004. Hepatic radiofrequency ablation – an overview from an engineering perspective. Proceedings of the 26th Annual International Conference of the IEEE EMBS.

Hanai T, 1960. Theory of the dielectric dispersion due to the interfacial polarization and its application to emulsions. Colloid & Polymer Science, 171, 1, 23-31.

Hilfer R, 1990. Geometric and dielectric characterization of porous media. Physical Review B, 44, 1.

Hoetink AE, Faes TJ, Visser KR, Heethaar RM, 2004. On the Flow Dependency of the Electrical Conductivity of Blood. IEEE Transactions on Biomedical Engineering, 51, 7.

Hu J, Klinich KD, Miller CS, Rupp JD, Nazmi G, Pearlman MD, Schneider LW, 2010. A Stochastic Visco0hyperelastic Model of Human Placenta Tissue for Finite Element Crash Simulations. Annals of Biomedical Engineering, Vol. 39, No. 2, 1074-1083.

Huang WH, Chui CK, Teoh SH, Chang SK, 2012. A multiscale model for bioimpedance dispersion of liver tissue. IEEE Trans Biomed Eng, 59(6),1593-7.

Huang WH, Chui CK, Kobayashi E, Teoh SH, Chang SKY, 2011. Multi-scale model for investigating the electrical properties and mechanical properties of liver tissue undergoing ablation. Int J Comput Assist Radiol Surg, 6(5), 601-607.

Jaffrin MY. Maasrani M, Le Gourrier A, Boudailliez B, 1997. Extra and intracellular volume monitoring by impedance during hemodialysis using Cole-Cole extrapolation. Medical and biological Engineering and Computing, 35, 266-270.

Jarnagin WR, Gonen M, Fong Y, DeMatteo RP, Ben-Porat L, Little S, Corvera C, Weber S, Blumgart LH, 2002. Improvement in perioperative outcome after hepatic resection. Analysis of 1803 consecutive cases over the past decade. Ann Surg, 4, 397–407.

Jiang J, Varghese T, Chen Q, Hall TJ, Zagzebski JA, 2007. Finite Element Analysis of Tissue Deformation with a Radiofrequency Ablation Electrode for Strain Imaging. IEEE Transactions on Ultrasonics, Ferroelectrics and Frequency Control, 54, 2, 281-289.

Jiao LR, Navarra G, Weber JC, Havlic R, Nicholls J, Habib NA, 2006. Radio Frequency Assisted Liver Resection: The Habib's Technique. Liver and Pancreatic Diseases Management, 31-37. 2006 Springer.

Khajanchee YS, Streeter D, Swanstrom LL, Hansen PD, 2004. A mathematical model for preoperative planning of radiofrequency ablation of hepatic tumors. Surg Endosc, 18, 696-701.

Kiss MZ and T Varghese, 2004. Viscoelastic characterization of in vitro canine liver tissue. IEEE International Ultrasonics, Ferroelectrics and Frequency Control Joint 50th Anniversary Conference, 2086-2089.

Kiureghian AD, Ke JB, 1988. The stochastic finite element method in structural reliability, Probabilist. Engrg. Mech. 3, 83–91.

Ko W, 2001. New method for Predicting Efficiency of Heating by Measuring Bioimpedance during Radiofrequency Catheter Ablation in Humans. Journal of Cardiovascular Electrophysiology. 12:7.

Kunii H and Kinouchi Y, 1998. Parameter Estimation of Lumped Element Circuit for Tissue Impedance. Annual International Conference of the IEEE Engineering in Medicine and Biology Society, 20, 3108-3111.

Larson TR, Bostwick DG, Corica A, 1996. Temperature-correlated Histopathologic Changes Following Microwave Thermoablation of Obstructive Tissue in Patients with Benign Prostatic Hyperplasia. 1996 Urology 47 (4)

Lazebnik M, Converse MC, Booske JH, Hagness SC, 2006. Ultrawideband temperature-dependent dielectric properties of animal liver tissue in the microwave frequency range. Physics in Medicine and Biology,51,1941-1955.

Lee RC, 1991. Physical Mechanisms of Tissue Injury in Electrical Trauma. IEEE Transactions on Education, 34, 3. 223-230.

Lin W, Buttemere C, Mahadevan-Jansen A, 2003. Effect of Thermal Damage on the In Vitro Optical and Fluorescence Characteristics of Liver Tissues. IEEE Journal of Selected Topics in Quantum Electronics, 9, 2, 162-170.

Lim D, Namgung B, Woo DG, Choi JS, Kim HS, Tack GR, 2010. Effect of Input Waveform Pattern and Large Blood Vessel Existence on Destruction of Liver Tumor using RF Ablation: Finite Element Analysis. Journal of Biomechanical Engineering, 132, 061003-1.

Liu J and Xu L, 1999. Estimation of Blood Perfusion Usng Phase Shift in Temperature Response to Sinusoidal Heating at Skin Surface. IEEE Transactions on Biomedical Engineering. Volume 46, 9.

Livraghi T, Goldberg SN, Monti F, Bizzini A, Lazzaroni S, Meloni F, Pellicanò S, Solbiati L, Gazelle GS, 1997. Saline-enhanced radio-frequency tissue ablation in the treatment of liver metastases. Radiology, 202, 205-210.

McGahan JP, Gu WZ, Brock JM, Tesluk H, Jones CD, 1996. Hepatic ablation using bipolar radiofrequency electrocautery. Acad Radiol, 3, 418-422.

McRae DA and Esrick MA, 1992. The dielectric parameters of excised EMT-6 tumors and their change during hyperthermia. Phys Med Biol, Vol 37, 11, 2045-2058.

Milicevic M and Bulajic P, 2008. Radiofrequency-Assisted Liver Resection Does not induce severe liver damage. World Journal of Surgery, 32: 1901-1902.

Moffit T, Baker D, Kirkpatrick S, Prahl S, 2002. Mechanical Properties of Coagulated Albumin and Failure Mechanisms of Liver Repaired with the Use of an Argon Beam Coagulator with Albumin. Journal of Biomedical Materials Research, 63, 722-728.

Montgomery RS, Rahal A, Dodd GD 3rd, Leyendecker JR, Hubbard LG, 2004. Radiofrequency Ablation of Hepatic Tumors: Variability of Lesion Size Using a Single Ablation Device. AJR, 182, 657-661.

Moor Instruments, moorVMS-LDF Probes. 2009. Retrieved January 2010, from http://www.moor.co.uk/products/monitoring/moorVMS-LDF/probes

Ni Y, Mulier S, Miao Y, Michel L, Marchal G, 2005. A review of the general aspects of radiofrequency ablation. Abdominal Imaging, 30, 381-400.

O'Rourke AP, Lazebnik M, Bertram HM, Converse MC, Hagness SC, Webster JG, Mahvi DM, 2007. Dielectric properties of human normal, malignant and cirrhotic liver

tissue: in vivo and ex vivo measurements from 0.5 to 20 GHz using a precision open-ended coaxial probe. Physics in Medicine and Biology, 52, 4707-4719.

Pellici R, Percibale A, Pittaluga M, Pasqualini M, Profeti A, Paroldi A, 2006. RF assisted Liver Resection: Experience of Italian Hepatic Surgery Unit. Liver and Pancreatic Diseases management, 39-41.

Pennes HH, 1948. Analysis of tissue and arterial blood temperatures in resting human forearm. Journal of Applied Physiology, 1:93-122.

Raicu V, Saibara T, Enzan H, Irimajiri A, 1998. Dielectric properties of rat liver in vivo: analysis by modeling hepatocytes in the tissue architecture. Bioelectrochemistry and Bioenergetics, 47, 333-342.

Roper R and Jones M, 2004. Benchmark Solution for the Prediction of Temperature Distributions During Radiofrequency Ablation of Cardiac Tissue. Journal of Biomedical Engineering, 126, 519-522.

Rupert N, Bharat S, Dewall R, Andreano A, Brace C, Jiang J, Sampson L, Zagzebski JA, Lee F, Varghese T, 2009. In Vivo Ultrasound Electrode Displacement Strain Imaging. IEEE International Ultrasonics Symposium Proceedings.

Sakamoto K, Sunaga R, Nakamura K, Sato Y, Fujii M, Kanai H, Tsuchida T, Ueno A, Kanai N, Hasegawa K, 1999. Study of the Relation between Fluid Distribution Change in Tissue and Impedance Change during Hemodialysis by Frequency Characteristics of the Flowing Blood. Annals of the New York Academy of Sciences, v 873, p 77-88.

Santago AC, Kemper AR, McNally C, Sparks KL, Duma SM, 2009. Freezing affects the mechanical properties of bovine liver. Biomed Sci Instrum, 45, l24-9.

Schwan HP, 1999. The Practical Success of Impedance Techniques from an Historical Perspective. Annals New York Academy of Science.

Schwan HP and Foster KR, 1980. RF-Field Interactions with Biological Systems: Electrical Properties and Biophysical Mechanisms. Proceedings of the IEEE, 68, 1.

Solazzo SA, Liu Z, Lobo SM, Ahmed M, Hines-Peralta AU, Lenkinski RE, Goldberg SN, 2005. Radiofrequency Ablation : Importance of Background Tissue Electrical Conductivity – An Agar Phantom and Computer Modeling Study. Radiology, 236, 495-502.

Southern J, Pitt-Francis J, Whiteley J, Stokeley D, Kobashi H, Nobes R, Kadooka Y, Gavaghan D, 2008. Review: Multi-scale computational modeling in biology and physiology. Progress in Biophysics and Molecular Biology 96 (2008) 60-89.

Stefanou G, 2009. The stochastic finite element method: Past, present and future. Comput. Methods Appl. Mech. Engrg. 198, 1031-1051.

Stippel DL, Brochhagen HG, Arenja M, Hunkemöller J, Hölscher AH, Beckurts KT, 2004. Variability of Size and Shape of Necrosis Induced by Radiofrequency Ablation in Human Livers: A Volumetric Evaluation. Annals of Surgical Oncology, 11(4), 420-425.

Smye SW, 2001. A mathematical comparison of two models of the electrical properties of biological tissues. Physics in Medicine and Biology, 46, 3.

Smye SW, Evans CJ, Robinson MP, Sleeman BD, 2007. Modelling the electrical properties of tissue as a porous medium. Physics in Medicine and Biology, 52, 7007-7022.

Taton G, Rok T, Rokita E, 2008. Temperature Distribution Assessment during Radiofrequency Ablation. IFMBE Proceedings 22, 2672-2676.

Thomsen S, 2009. Targeted Thermal Injury: Mechanisms of Cell and Tissue Death. Energy-based Treatment of Tissue and Assessment V, Proc. Of SPIE Vol 7181

Tranberg KG, 2004. Percutaneous Ablation of Liver tumours. Best Practice & Research Clinical Gastroenterology, 18, 1, 125-145.

Vasilkoski Z, Esser AT, Gowrishankar TR, Weaver JC, 2006. Membrane electroporation: The absolute rate equation and nanosecond time scale pore creation. Phys Rev E Stat Nonlin Soft Matter Phys, 74(2 Pt 1), 021904.

Walker DC, Brown BH, Hose DR, Smallwood RH, 2000. Modelling the electrical impedivity of normal and premalignant cervical tissue. IEE, 36, 19.

Walsh JT and Deutsch TF, 1989. Pulsed CO2 Laser Ablation of Tissue: Effect of Mechanical Properties. IEEE Transaction on Biomedical Engineering, 36, 12, 1195-1201.

Whitathey T, Stuchly MA, Stuchly SS, 1982. Measurement of RF Permittivity of Biological Tissues with an Open-Ended Coaxial Line: Part I. IEEE Transactions on Microwave Theory and Techniques, 30, 1.

Wierwille J, McMillan A, Gullapalli R, Desai J, Chen Y, 2010. Quantitative Characterization of Radiofrequency Ablation Lesions in Tissue Using Optical Coherence Tomography. IFMBE Proceedings 32, 485-488.

Yang DS, Converse MC, Mahvi DM, Webster JG, 2007. Expanding the Bioheat Equation to Include Tissue Internal Water Evaporation During Heating. IEEE TBME, 54, 8, 1382-1388.

Yang L, Wen R, Qin J, Chui CK, Lim KB, Chang S, 2010. A robotic system for overlapping radiofrequency ablation in large tumor treatment, IEEE-ASME Transactions on Mechatronics, 15(6), 887-897

Yasuno E, Zhao X, Kinouchi Y, Morimoto T, 2006. Parameter estimation method of the biological tissue equivalent circuit model for local EIT. International Conference of the IEEE Engineering in Medicine and Biology Society, 4.

PUBLICATIONS

Journal Publications

1) **Huang WH**, Chui CK, Kobayashi E, Teoh SH, Chang SKY, 2011. Multi-scale model for investigating the electrical properties and mechanical properties of liver tissue undergoing ablation. International Journal of Computer Assisted Radiology and Surgery, 6(5), 601-607.
2) Chang SKY, Hlaing WW, **Huang WH**, Chui CK, 2011. Integrated ablation and division device for liver resection. HPB, 13(3) , 158-160.
3) **Huang WH**, Chui CK, Teoh SH, Chang SKY, 2012. A multiscale model for bioimpedance dispersion of liver tissue. IEEE Transaction of Biomedical Engineering, 59(6), 1593-1597.
4) Florence Leong, **Huang WH**, Chui CK, 2012. Modeling and Analysis of Coagulated Liver Tissue and its Interaction with a Scalpel Blade. Medical & Biological Engineering & Computing. Accepted for publication
5) **Huang WH**, Chui CK, Chang SKY, 2011. Minimizing Invasiveness of Liver Resection using an Integrated Tissue Ablation and Division Device with Blood Flow Sensing. ASME Journal of Medical Devices. Minor revision, and revised manuscript submitted.
6) **Huang WH**, Chui CK, 2012. Stochastic Finite Element Method for Large Tumor Radio-frequency Ablation Planning. IEEE Transaction of Biomedical Engineering. Submitted.

Book Chapter

1) **Huang WH**, Chui CK, 2012. Connecting Tissue Injury, Temperature and Mechanical Properties. In: Soft Tissue: Composition, Mechanisms of Injury and Repair, Nova Science Publishers, Inc. (Editors: Antonio J. Chavez Ruiz and Jose M. Alvarez Mendoza)

Conferences

1) **Huang WH**, Chui CK, Kobayashi E, Chang SKY, 2009. Modeling of Liver Tissue for Investigation of Tissue Properties Changes during Radio-Frequency Ablation. 5th Asian Conference on Computer Aided Surgery (ACCAS 2009), 3rd to 4th July, Taichung, Taiwan.
2) **Huang WH,** Chui CK, 2012. A Radio-Frequency Ablation Planning System using Stochastic Finite Element Method. IEEE/SICE International Synopsium on System Integration (SII 2012), 16th to 18th December, Fukuoka, Japan.